84-34330

Baseline Performance and Emissions Data for a Single-Cylinder, Direct-Injected, Diesel Engine

Robert A. Dezelick, John J. McFadden,
Lloyd W. Ream, and Richard F. Barrows
National Aeronautics and Space Administration
Lewis Research Center

September 1984

DISCLAIMER

This report was prepared as an account of work sponsored by an agency of the United States Government. Neither the United States Government nor any agency thereof, nor any of their employees, makes any warranty, express or implied, or assumes any legal liability or responsibility for the accuracy, completeness, or usefulness of any information, apparatus, product, or process disclosed, or represents that its use would not infringe privately owned rights. Reference herein to any specific commercial product, process, or service by trade name, trademark, manufacturer, or otherwise, does not necessarily constitute or imply its endorsement, recommendation, or favoring by the United States Government or any agency thereof. The views and opinions of authors expressed herein do not necessarily state or reflect those of the United States Government or any agency thereof.

Printed in the United States of America

Available from
    National Technical Information Service
    U.S. Department of Commerce
    5285 Port Royal Road
    Springfield, VA 22161

NTIS price codes[1]
    Printed copy: A03
    Microfiche copy: A01

[1]Codes are used for pricing all publications. The code is determined by the number of pages in the publication. Information pertaining to the pricing codes can be found in the current issues of the following publications, which are generally available in most libraries: *Energy Research Abstracts (ERA); Government Reports Announcements* and Index *(GRA* and I); *Scientific and Technical Abstract Reports (STAR);* and publication, NTIS-PR-360 available from NTIS at the above address.

ERRATA

NASA Technical Memorandum 83638
DOE/NASA/50194-38

BASELINE PERFORMANCE AND EMISSIONS DATA FOR A SINGLE-CYLINDER,
DIRECT-INJECTED, DIESEL ENGINE

Robert A. Dezelick, John J. McFadden,
Lloyd W. Ream, and Richard F. Barrows
September 1984

Cover, title page, and report documentation page: The Technical Memorandum number should be TM-86873.

Figure 21: In part (a), the Duration label should read Duration, 22°; in part (b), Duration, 25°; in part (c), Duration, 30°; and in part (d), Duration, 34°. Also, in figure 21(c), 232 g/kW-hr BSFC should appear in the lower right corner. In the figure 21 legend, the fuel quantity should be 140 mm^3/cycle.

Figures 37 to 41: In the legends, delete inlet air temperature, 34 to 37 °C; add inlet air pressure, 262 kPa.

Figures 42 to 45: The key should read Inlet air pressure, kPa. The ordinate scale label for the second graph from the bottom should read CO emission, percent.

Figure 56: Key symbols (top to bottom) should be △, □, ◇. The top value on the ordinate scale should be -.05.

Baseline Performance and Emissions Data for a Single-Cylinder, Direct-Injected, Diesel Engine

Robert A. Dezelick, John J. McFadden,
Lloyd W. Ream, and Richard F. Barrows
National Aeronautics and Space Administration
Lewis Research Center

September 1984

BASELINE PERFORMANCE AND EMISSIONS

DATA FOR A SINGLE CYLINDER, DIRECT

INJECTED, DIESEL ENGINE

Robert A Dezelick, John J. McFadden,
Lloyd W. Ream, and Richard F. Barrows
National Aeronautics and Space Administration
Lewis Research Center
Cleveland, Ohio 44135

SUMMARY

The Department of Energy (DOE), Division of Transportation Energy Conservation, has established several broad programs aimed at reducing highway fuel consumption. Within the Heat Engine Highway Vehicle Systems Program is a subproject that addresses control technology for the reduction of particulate and gaseous emissions of diesel engines. Program management for this project has been delegated to the National Aeronautics and Space Administration (NASA), Lewis Research Center .

The research engine tested was a 120-mm-bore by 120-mm-stroke, single-cylinder open-chamber, four-stroke-cycle, diesel engine with a 17.29 compression ratio. A modular engine instrumentation system (MEIS), developed at NASA Lewis, was used to provide a real-time computation of the indicated mean effective pressure developed from the pressure-volume diagram. Baseline performance data were developed and compared with data supplied by the manufacturer, inlet air pressure and temperature effects were evaluated, and exhaust emissions data were collected under various operating conditions.

Baseline exhaust emissions data were developed for CO, HC, NO_x, total particulate mass, the soluble organic fraction of the total particulates, and exhaust smoke opacity. Emissions of CO increased with speed due to lower volumetric efficiency at higher speeds. Hydrocarbon emissions and total brake specific particulate matter were proportional to engine speed for constant fuel injected quantities and inversely proportional to load. Oxides of nitrogen values decreased with an increase in engine speed from 2500 to 3000 rpm for constant fuel quantities, and decreased between 1500 and 3000 rpm for higher fuel quantities (120 to 140 mm^3/cycle).

The inlet air pressure and temperature to the engine were changed to simulate the effects of supercharging and turbocharging. Optimum engine performance, based on specific fuel consumption and mean effective pressure, was obtained with an inlet air pressure of 329 kPa. Lowest exhaust emissions and smoke opacity were obtained with inlet air pressures of 372 kPa or higher. The inlet air temperature effects at 2000 rpm indicate that mean effective pressure improvements on the order of 8 to 13 percent can be obtained with 37.8° C inlet air temperature compared with 107° C. This improvement is indicative of the benefit to be derived from aftercooler/intercooler control techniques on turbocharged engines.

A mathematical relationship was developed to predict total measured particulate matter as a logarithmic function of exhaust smoke opacity plus total exhaust hydro-carbons. The calculated particulate emissions were used to assess the effect of inlet air pressure on particulate formation.

The MEIS independently assesses real-time mean effective pressures for the upper loop of the pressure-volume diagram , the lower pumping loop , and the sum of the two loops. Real-time values of actual FMEP are shown to be 19 to 29 percent higher for the engine under load (at fuel quantities of 60 to 140 mm^3/cycle, respectively) than for a motored engine at rated speed (3000 rpm). However, motored friction, in the normal sense, includes both pumping and fricion mean effective pressure. Real-time values by this definition were also assessed under different operating conditions. The results of this analysis indicate that FMEP + PMEP for an engine under load (140 mm^3/cycle), at rated speed (3000 rpm), is about the same as the motored engine value, but as much as 15 percent lower than the motored engine value at 1500 rpm. It was determined that positive work can be accomplished from the pumping loop by increasing the inlet air pressure, by decreasing the exhaust backpressure, or by a combination of both methods. For one example, a 13 percent gain in performance was obtained by increasing the inlet air pressure from 262 to 414 kPa and by reducing the exhaust backpressure from 207 to 124 kPa.

INTRODUCTION

The Department of Energy (DOE), Division of Transportation Energy Conservation, has established several broad programs aimed at reducing highway fuel consumption. One such program is the Heat Engine Highway Vehicle Systems Program. Within that program is a subproject which addresses control technology for the reduction of particulate and other emissions from diesel engines.

One of the NASA programs underway at Lewis is directed toward reducing fuel consumption and exhaust emissions for lightweight diesel aircraft engines for general aviation use. One accomplishment of this program has been the construction and development of a fully instrumented, single-cylinder, diesel engine test facility. Because of the similarity in objectives between advanced automotive and aircraft diesel engine technology, it was technically feasible and cost effective to combine selected NASA research efforts with those of the Department of Energy (DOE).

The data and technology developed in this project are intended to provide the basic emissions and performance technologies that will help DOE to independently assess the environmental acceptability of the open-chamber diesel engine for general highway operation and to show the potential value for tested control concepts in future regulatory decisions.

This control technology part of the program encompasses the testing and evaluation of a single-cylinder, open-chamber, diesel, test engine. Tests were conducted with the objective of accumulating repeatable baseline data and assessing the effects of various input variables on engine performance and exhaust emissions. A secondary objective was to explore the capability and accuracy of different instruments as measurement techniques.

The single-cylinder research engine (SCRE) test facility at Lewis, was put into an operational status, and baseline performance data were collected and compared with data provided by the engine manufacturer. Inlet air pressure and temperature were varied to demonstrate the best combination of these variables for minimum specific fuel consumption, exhaust emissions, and particulates. A mathematical expression was developed to predict the effect of engine operating parameters on the formation of total particulates.

A Modular Engine Instrumentation System (MEIS), developed at Lewis, for real-time measurements of mean effective pressure, was modified to provide independent assess-

2

ment of the power loop (upper) and the pumping loop (lower) on the single-cylinder four-stroke cycle engine. This provided the capability to independently assess friction and pumping losses under loaded engine conditions and to more accurately evaluate the effects of such control strategies as turbocharging. Friction and/or pumping losses under loaded engine conditions were also compared with similar data developed by the more conventional motoring procedure.

APPARATUS AND PROCEDURE

Test Facility

The single-cylinder diesel engine test stand installation is shown in figure 1. The engine is coupled to a 22-kW motoring and a 93-kW absorbing dynamometer. Engine cooling is controlled by a closed-loop water system with an engine driven pump. On the cooling loop is a heat exchanger that uses cooling tower water. Fuel is supplied to the engine from a gravity-feed float-controlled tank, to an in-line, fuel injection pump. Fuel is supplied to the gravity tank from an outdoor source consisting of a 0.189-m^3 (50-gal) drum with an appropriate filtering, pumping, and measuring system.

Inlet air system. - The inlet air system uses surge tanks to dampen flow pulses and provides air from a 690-kPa plant source. Conditioning systems provide for air pressures from ambient to 690-kPa and temperatures from ambient to 121 °C, with specific humidities from approximately 0.09 g H_2O/g dry air to saturation.

Exhaust system. - The exhaust system incorporates a remotely controlled valve that is used to control the engine backpressure and to simulate the effects of a turbocharger. For a majority of the tests conducted, the backpressure was held at 80 percent of the inlet pressure. Surge tanks are used in the exhaust system to reduce the pulses from the single-cylinder engine.

Engine Description

Engine data. - The following table describes the single-cylinder test engine.

Bore, mm (in.)	120 (4.724)
Stroke	120 (4.724)
Percent first-order balancing	100
Piston displacement, cm^3 (in^3)	1357 (82.8)
Number of piston rings	4
Clearance volumes, cm^3	
Combustion cavity in the piston,	63.2
Valve pockets in cylinder head	
Intake	2.3
Exhaust	2.0
Quartz transducer cavity	0.4
Injection nozzle cavity	0.5
Piston to head clearance	14.92
Total clearance volume	83.32
Compression ratio: (1357 + 83.32)/83.32	17.29
Four valve cylinder head: 2-intake, 2-exhaust and 2-camshafts	
Cylinder head thickness gasket, mm	1.6
Rocker arm ratio	1:1.5

Valve lash, 1 mm

    Intake 0.4

    Exhaust 0.6

    Approximate lift, ... 9.7

Fuel injection line:

    Outside diameter, mm 6

    Inside diameter, mm 2.2

    Length, mm 600

Nozzle holder opening pressure, MPa (psi) 25.5 (3700)

Nozzle

    Number of holes 5

    Hole diameter, mm 0.36

    Length to diameter ratio, L/D 2.8

    Sac volume, mm^3 . . . . 3.6

    Spray angle, deg 150

Nozzle valve and seat diameters, mm . . . . 6 by 3.5

      Fuel injection equipment. - The injection pump has a four-cylinder case. Elements 3 and 4 are blank, and 1 and 2 are parallel and working.

The two injection pumps used the same cam profile (fig. 2): One has two 10-mm-diameter plungers, with delivery valve retraction volumes of 120 mm^3; the other has 9-mm-diameter plungers, with delivery valve retraction volumes of 70 mm^3.

      Injection timing was controlled by a motor driven timing device, where one revolution of the timing device corresponds to a variation in injection timing of 1° of engine crank angle. The total injection timing range available is approximately 20° of crankshaft rotation.

      Lubricating oil system. - The lubricating oil system has a capacity of 14 liters (14.8 qt) and contains an engine-driven oil pump. Oil temperature control is provided.

Exhaust Analysis System

Emissions sampling system. - The engine exhaust gas sampling system has provision for exhaust gas analysis and particulate measurement. For exhaust gas analysis, a continuous sample is drawn from the pressurized section of the exhaust line. The gas flows through sample lines (maintained at 190° C) to the gas analysis instruments. Particulate and gaseous emissions were measured for single modes of operation according to the EPA Federal Test Procedure (FTP), Heavy Duty Engines, Code of Federal Regulations (CFR), Title 40, Part 86, Subpart D, Section 86.345-79.

      A schematic of the sampling transfer and data handling system is shown in Figure 3(a). When not sampling, the sample line is purged using air. The sample temperature is maintained within allowable limits in the transfer system in order to maintain the sample's integrity.

      The exhaust gas analysis instrument facility flow diagram is shown in figure 3(b). The system is capable of measuring the concentrations of carbon monoxide (CO), carbon dioxide (CO_2), nitric oxide (NO), total oxides of nitrogen (NO_x), total hydrocarbons (HC), and oxygen (O_2). Table I(a) lists information for the exhaust gas analysis instruments used.

Chart recorders are provided on the gas analysis instrument panel as well as panel analog meters. The recorders are used to monitor stability when changing from one test condition to another.

Calibration. - Zero and span gas calibrations are traceable to the National Bureau of Standards. The calibration system consists of 16 high-pressure gas cylinders fitted with pressure-reducing regulators. The gas cylinders are enclosed in a cabinet provided with a hood and an induced draft fan. The fan discharge is ducted through the outside wall, providing dilution and removal of any leakage gas during calibration. The calibration gases are fed to a calibration gas panel located behind the gas analysis instruments in the control room. Stainless-steel tubing is used between the cylinders and the calibration panel. The panel is setup to provide a known calibrated gas for each instrument. Flexible Teflon lines are used between the calibration panel and the instruments. The zero gas used for measurement of NO/NO_x, CO, CO_2 and O_2 is nitrogen. Plant air is passed through a catalytic device, which then provides the HC-free air used as the zero gas for the measurement of total HC. The flow schematic for the exhaust gas analysis system is shown in figure 5.

Sixteen span gas cylinders provide a range of known concentrations so that calibration can be accomplished at various operating conditions. Table II shows the concentrations of the span gas bottles available for use in the test cell.

Particulate sampling system. - The equipment for particulate sampling consists of a dilution tunnel, sample probes, filter cassette sampling system, vacuum pump, sample flowmeter, and a control unit. A schematic of the dilution tunnel and equipment is shown in figure 4. The 25.4-cm-diameter and 305-cm-long tunnel provides for complete mixing of the dilution air and exhaust gas before sampling. The dilution air enters the tunnel from the test cell, passing through an impregnated filter for removal of hydrocarbons. After sampling, the air and exhaust pass through a heater to a positive displacement blower, and, finally, exhaust through the roof of the test cell. The purpose of the heater is to maintain the inlet conditions to the blower. The blower speed may be varied and is used to control the amount of air diluting the exhaust. Tunnel flow is adjusted to keep the sampling temperature below 52° C (125° F). An air dilution flow of eight times the exhaust flow is normally enough to keep the temperature below 52° C (125° F).

There are two probes at the end of the 305-cm section to pick up the exhaust. The dilute gas passes through either the particulate filter cassette or through a bypass filter. An automatic flow controller maintains an established flow rate through the probe and filter. The specifications and operating guidelines are presented in table III.

The sampling filters were conditioned in a humidity chamber for 24 hr before weighing and particulate collection. After collection, the filters were again stored in a humidity chamber to stabilize mass to the original humidity before weighing. Total particulate mass from each test was determined by adding the particulate mass from both the primary and backup filters. A representative number of filters were placed in glass Soxhlet microextractors, and the soluble organic fraction (SOF) was extracted using dichloromethane solvent. The samples were then reconditioned in the humidity chamber and reweighed. The difference in mass between the total particulate matter (TPM) and the soluble organic material (SOM) represents the unextractable residue, or solid mass fraction (ref. 1).

The microbalance used for this measurement is accurate to ±0.01 mg. The net weight of the TPM, the sample probe flow volume that passed through the filter, and the sample

5

time are recorded manually and entered into the data collector system for processing. The soluble organic and solid mass fractions are also manually recorded.

Instrumentation

The engine test operators console and engine instrumentation panel are shown in figure 5. Some of the instruments used are as follows:

(1) In-line light extinction meter for measuring smoke opacity.

(2) Filter sampling smoke meter.

(3) Blow-by meter, used to monitor the condition of the engine and measure crankcase gases vented to the atmosphere.

(4) Linear, differential, inductive type valve lift transducer, used to determine the position of the valves (inlet and exhaust).

(5) Linear, differential, inductive type needle lift transducer, used to monitor the position of the valve in the nozzle.

(6) Piezoelectric, water cooled, transducer, used to measure cylinder gas pressure (24.8 MPa max.).

(7) Temperature controlled, mirrored, photoelectric sensor, used to obtain dew point.

(8) A modular engine instrument system (MEIS) (ref. 2), used to provide the following:

(a) Pressure-volume diagram of the thermodynamic cycle, on an oscilloscope display, which is updated every cycle. The modular unit displays indicated mean effective pressure (IMEP). Associated modules display peak cylinder pressure, in engineering units, which are updated each cycle, and the degrees before or after top dead center (TDC) where peak pressure occurs. These data are transmitted to the data acquisition system.

(b) Another unit provides the log function of cylinder pressure and volume on an oscilloscope display. A Polaroid picture, or the display itself, may be measured with a protractor. The tangent of the angle then provides an on-line value of the polytropic exponent for any portion of the pressure volume diagram.

(c) Another module displays the peak injection pressure and the angle before top dead center (BTDC) where the peak pressure occurs.

(d) Also available as a module is a unit that will accept four parameters such as cylinder pressure, injection pressure, IMEP, etc. This unit will sample and store up to 200 cycles and displays the mean and standard deviation values. The four parameters can be shown on an oscilloscope as a series of vertical bars (one per cycle).

The major measured parameters are listed in table IV. In general, the overall accuracy of each individual data point is 0.5 percent of the full scale value of the transducer.

All instrumentation is connected to a data system known as ESCORT which provides a wide variety of computerized data services to the research facilities at Lewis. A remote acquisition microprocessor (RAMP), located in the test facility, serves as an interface between the facilities instrumentation and monitoring devices. A minicomputer performs online calculations and outputs engineering unit displays on cathode ray tubes (CRT's) in the test facility.

Selected portions of the data can be recorded by a signal to the minicomputer. This then passes the data to a collector system which records the data on magnetic tape (legal record tape) and passes the data to the main computer for final processing. Hard copy data can be printed out at the test facility from any of a number of CRT displays that have been previously programmed. The time, date, and a precision digital barometer attached to the data collector are read onto the tape before a data record. The ESCORT system also provides digital signal conditioning. The facility is placed in a null position and zero data are taken. Calibration resistors are automatically switched in, and the span data are taken. The correction factor for each channel is then calculated, stored, and recorded on the data collector for use in the central data-reduction system. These values are checked each test day against a baseline set of values for drift exceeding 2 percent.

Calculations

Calculations in this report are based on standard-day conditions of 100 kPa and 15° C. The water correction factor, calculated air to fuel ratio, etc., calculations were developed for use in CFR, Title 40, Part 87, Subpart E; exhaust emissions (new and in use aircraft piston engines). These, in general, agree with Title 40, Part 86, Subpart D, Section 86.345-79 emission calculations for heavy-duty diesel engines.

Test Procedure

Before starting a test, all instruments were calibrated. Pressure transducers were automatically calibrated by the ESCORT data system. The data system was brought on line, and the test cell brought to the null condition; that is, no flow, with the pressure transducers at atmospheric pressure. By communicating with the minicomputer via a typewriter and push buttons, zeros were recorded in the data system, and the instrument spans were recorded (resistance calibrations). The data system was then returned to the data mode and digital readouts were updated. The engine was then started and brought to operating temperature. For this series of tests, the engine water temperature was held at 77.8° C (172° F) and the engine oil temperature at 91.1° C (196° F). A test point was then established by setting the desired air inlet pressure and temperature and the proper exhaust pressure. Data points were taken at speeds of 1000 to 3000 rpm in increments of 500 rpm. A dynamometer load was then set to establish equal increments of fuel flow per cycle from 40 to 200 mm^3/cycle, with 35 percent smoke opacity being the normal cutoff point. Injection timing was then adjusted to the desired setting (normally to maximum power), with the limits being a maximum IMEP of 2.5 MPa at 2000 rpm, or a maximum IMEP of 2.0 MPa at 3000 rpm.

When all values are stabilized, including emission data, a data point was taken. Five scans of data were taken for all parameters with approximately 1 sec between scans. When the data collector has transmitted the data from the data tape to the computer, the operator was notified by a typed signal which gives the exact time of transmittal and the run number. Computer printouts of the data were received the next day, and gave an average (for the five scans), minimum, and maximum values, in both millivolts and engineering units, for all the data channels. The printouts also tabulated results of engine

flows, emissions, engine performance, and heat balances. Data were saved when requested for plotting of various parameters.

TEST RESULTS

Acceptance Testing

The curves shown in figure 6 are the initial test results for the single-cylinder test engine in the Lewis facility compared with the engine manufacturer's data. The difference in values is attributable to the variations in fuel specifications, piping arrangements, transducer sensor locations, etc. The volumetric efficiency curves (fig. 7) demonstrate the effects of inlet manifold resonance which occurred at 2000 rpm. This appears to be a desirable feature for this engine when operated at this speed, but the inlet manifold was modified (enlarged) so that other effects would not be masked.

Data derived from the various test runs of the engine facility are used in many ways. The primary purpose is to establish good, repeatable baseline data so that the effects of air, fuel, or hardware changes to the engine can be recognized from the data. A second purpose is to establish or verify the accuracy of various instruments or measurement techniques being proposed or investigated. The third purpose is to provide research investigators with the data necessary to compare the theoretical with the actual values, while visually observing how changes affect or limit theoretical goals. Many of the curves provided are for the use in follow-on investigations and provide the background or baseline data required to show trends.

Inlet Pressure Effects

The inlet air pressure of the engine was changed while maintaining the exhaust pressure at a 1.25 inlet to exhaust pressure ratio PI/PE. This value was used throughout the program to simulate a typical turbocharger unless stated otherwise. Fuel injection timing was set for maximum BMEP. Figure 8 shows that the air-to-fuel equivalence ratio ((A/F actual)/(A/F stoichiometric) decreased with increased load at any fixed inlet pressure.

Figures 9 to 12 show the various performance parameters as they are affected by changes in inlet air pressure. It can be observed that optimum engine performance (brake mean effective pressure (BMEP), brake power output (BPO), brake specific fuel consumption (BSFC), and brake thermal efficiency) occurs with approximately a 329 kPa inlet air pressure, while maintaining the pressure ratio at 1.25, and inlet air temperature at $27\pm5°$ C. As shown in figure 9, increases in inlet air pressure from 329 to 414 kPa do not significantly affect engine BMEP for any of the fuel quantities shown. Figure 10 shows that brake power increased 30 percent by raising the inlet air pressure from 193 to 329 kPa for 140 mm^3/cycle. Figures 11 and 12 show that the lowest BSFC and highest brake thermal efficiency values occur at an inlet air pressure of 329 kPa. Figure 13 shows the effect of speed on peak cylinder gas pressures with increasing load at different inlet air pressures. Injection timing was adjusted to maintain maximum cylinder pressure within recommended design limits.

Figure 14 shows peak cylinder gas temperature plotted against BMEP for different fuel quantities and five inlet air pressures at 2000 rpm. A computer equilibrium subroutine for hydrocarbon fuels was used to calculate the peak cylinder temperature, or the total equilibrium combustion product temperature (TECPT). Peak cylinder gas temperatures decrease with increased inlet air pressure for constant fuel quantities as shown for 2000 rpm operation. Figure 15 shows the effect of speed on peak cylinder gas tempera-

ture at different loads for each of five levels of inlet air pressure. Figure 16 shows similar effects of inlet air pressure on exhaust gas temperature for different speeds and loads.

Figure 17 shows how increased A/F's affect BMEP for different fuel quantities and engine speeds. Optimum performance (maximum BMEP) occurs at A/F's greater than 30.

Figure 18 shows BSFC plotted against A/F for different inlet air pressures. Optimum BSFC occurred at A/F's > 30. Best overall fuel consumption at both speeds was obtained with an inlet air pressure of 329 kPa. Figure 19 shows the same effect in terms of brake thermal efficiency at 2000 rpm. Figure 20(a) shows that the sensitivity of peak cylinder pressure for inlet air pressures of 329 kPa and greater, required retarded timing at the higher loads (A/F < 40) in order not to exceed the maximum design limit. Figure 20(b) shows peak cylinder temperature as an inverse function of A/F and proportional to load or fuel quantity.

Fuel Injection Timing Effects

The data obtained from the photographs of the oscilloscope traces (fig. 21) demon strated the increase in the duration of injection as a function of speed, ranging from 22° at 1500 rpm to 34° at 3000 rpm for 140 mm^3/cycle. The average duration was 2.1 msec, and the average needle lift rise time was 0.4 msec. From interpretation of the pressure diagrams (fig. 25) and from the camshaft analysis (fig. 3), it can be shown that (by calculations) over 90 percent of the fuel is injected by expansion of the fuel after the point of peak injection pressure. This behavior is similar to that of an accumulator fuel injection system. The result is a decreasing rate of injection that is neither congruent with nor controlled by the pump camshaft profile.

The oscillograms of figure 21 also illustrate how the peak cylinder gas pressure was kept below allowable limits by adjusting the timing, with respect to speed while maintain ing the best BSFC. The dynamic effects of the injection system were exemplified by injection pressure increases with increases in engine speed; that is, 41.6 MPa at 1500 rpm to 65.7 MPa at 3000 rpm. For these curves static timing merely refers to a reference point for the start of plunger lift in the injection pump. The approximate relationship of static timing with the open position of the nozzle valve is shown in figure 22. This open position of the nozzle valve occurred at the approximate point in the cycle where peak injection pressure occurs and is the reference used in this report for dynamic injection timing.

Figure 23 shows the injection and ignition delay variables for five fuel quantities and four speeds with optimum injection timing. Figures 24 and 25 show the effect of injection timing on part load performance (BMEP and BSFC, respectively) at three speeds.

Inlet Temperature Effects

Volumetric efficiency can be a misleading parameter when evaluating supercharged engines. By definition, volumetric efficiency is the ratio of the actual weight of air inducted by the engine on the intake stroke to the theoretical weight of air that should have been inducted by filling the piston displacement volume with air at atmospheric temperature (ref. 3). Volumetric efficiency, by this definition, can be a useful reference. However, with supercharged engines, the denominator becomes a variable determined by actual inlet manifold conditions. The ratios might suggest that volumetric efficiency

increases with increased manifold temperature. This is a mathematical anomaly since the inlet air mass charge is less with higher inlet air temperatures (fig. 26).

For parametric analyses, BMEP and BSFC are more meaningful indicators of overall engine performance. Improvements in BMEP on the order of 8 to 13 percent were obtained with reductions in inlet air temperature at 2000 rpm (fig. 27). Slightly less improvement is shown for 2500 rpm. Figure 28 shows improvements in BSFC for the same conditions. These sets of curves are indicative of the benefits to be derived from aftercooler/intercooler control techniques on turbocharged engines. In general, optimum injection timing is not influenced by changing the inlet air temperature for lowest BSFC values.

Exhaust Emissions - Baseline Results

Table V summarizes the mean values for baseline exhaust emissions with injection timing set for optimum engine performance (minimum BSFC and maximum BMEP). Inlet air pressure was set for 262 kPa and inlet air temperature for 34° C. Figures 29 to 32 show baseline brake specific CO, HC, NO_x, and total particulate emissions plotted against BMEP, engine speed, and A/F. The CO emissions increase with speed at the higher loads because of lower volumetric efficiencies. Lowest CO values occur with fuel quantities of 100 mm^3/cycle in the range of 35 to 48 A/F. As shown in figure 30, HC emissions decrease with increasing load, or lower A/F, but tend to increase with speed for most fuel quantities. The brake specific oxides of nitrogen (BSNOX) emissions (fig. 31) decrease with increased speed between 2500 and 3000 rpm for fuel quantities between 60 and 140 mm^3/cycle. For higher fuel quantities of 120 and 140 mm^3/cycle, there is also a general decrease in BSNOX emissions between 1500 and 3000 rpm. As shown in figure 32, total measured brake specific particulate matter (BSPM) decrease with increas- ing load between 1500 and 3000 rpm. This reduction in total measured particulates direc- tionally follows the same trend shown for hydrocarbons with increasing load.

In-line optical smoke extinction meters were used to determine exhaust smoke opacity and to calculate total particulate matter as determined by the method developed and described in references 4 and 5. The exhaust volumetric flow rate was corrected for temperature at the smokemeter to determine actual volumetric flow rates. Calculated BSPM was determined from

$$BSPM = \frac{(Cm)(EXVOL)(10^{-3})}{kW}$$

where

$$Cm = \frac{-122}{L} \ln\left(1 - \frac{N}{100}\right) mg/m^3$$

and where

L mean wave length of lens of smoke meter (0.146 m)
N opacity, percent
EXVOL exhaust volumetric flow rate, m^3/hr

Calculated BSPM for four engine speeds and five loads are compared with measured BSPM in figure 33. The data are scattered and no correlative trends are apparent. The total particulate mass, however, comprises complex mixtures of solid and liquid com- pounds. The solid fraction is primarily carbonaceous matter, and the liquid fraction is

10

mostly organics and sulfates. As postulated by Greeves (ref. 6), total particulate mass contains the black soot formed in the high-temperature fuel-rich regions of the diffusion phase of burning and that fraction of the total HC mass emission which condenses at the particulate sampling filter. Total particulate then becomes mostly a function of both smoke and HC emissions. Calculated BSPM is shown in figure 34 plotted against smoke opacity. A least squares linear regression was performed to produce the following relationship between calculated BSPM, considered as the solid fraction of total particulates, and smoke opacity:

$$BSPM_{calc} = 0.08(\text{percent opacity}) + 0.06$$

With this highly boosted engine (262 kPa inlet air pressure), many of the smoke opacity readings are extremely low, less than 5 percent, which is the threshold of visibility. Consequently, the correlation is not exact, but the trend is apparent that smoke opacity and calculated BSPM are more functions of the solid fraction of total particulates than of total particulates. The soluble organic mass fraction (SOF) is shown in figure 35 plotted against brake specific hydrocarbon emissions. The calculated SOF shown for this plot was determined by subtracting the calculated BSPM (a logarithmic function of smoke opacity) from the measured total particulate matter. This plot produced the following relationship between the calculated SOF and BSHC:

$$SOF_{calc} = 0.80 \ BSHC - 0.83$$

These two calculated expressions can be combined to produce the following:

$$BSPM_{meas} = BSPM_{calc} + SOF_{calc}$$

$$= 0.08 \ (\text{percent opacity} + 10 \ BSHC) - 0.77$$

The results of these combined expressions show better agreement when total measured particulates are compared with particulates calculated as a function of both exhaust smoke opacity and exhaust hydrocarbons (fig. 36). Test points include four engine speeds and five loads at each speed.

Exhaust emissions - inlet air temperature effects with variable timing

Figures 37 to 41 show the effect of inlet air temperature on fuel consumption, BSNOX, brake specific hydrocarbon (BSHC), and brake specific carbon monoxide (BSCO), for five fuel quantities at 2500 rpm. The effects of three injection timings are shown for 2500-rpm engine speed and 262-kPa inlet air pressure. The lowest inlet air temperature generally produced the lowest BSNOX, BSCO, and BSFC. Retarded injection timing showed more consistent trends in reduction of BSNOX than for other gaseous emissions, but with significant penalties in BSFC.

Exhaust Emissions - Inlet Air Pressure Effects

Figures 42 to 45 show the effect of inlet air pressure on smoke opacity and gaseous emission concentrations at four speeds. The lowest level of emissions and smoke opacity generally occurs with inlet air pressures at or greater than 372 kPa, while maintaining an inlet to exhaust pressure ratio of 1.25. Injection timing was set for optimum performance, that is, lowest BSFC and highest BMEP for each speed. Total measured particulate data were not collected for this series of tests. Figure 46 was constructed on the basis of

11

calculated brake specific particulates (BSPM) to establish the effect of increased inlet air pressure on particulates. Calculated BSPM is postulated to be a function of exhaust smoke opacity (solid fraction) and BSHC (soluble organic fraction), as previously described and shown in figure 36. Figure 46 shows that particulates are a function of A/F as influenced by inlet air pressure and that total particulates can be held to a minimum for A/F's greater than about 35 at 3000 rpm, 40 at 2500 rpm, 45 at 2000 rpm, and 50 at 1500 rpm. Particulates tend to increase below these A/F thresholds and demonstrate the potential for supercharging techniques to control particulates.

Exhaust Emissions - Jet A Fuel

Several tests were conducted with Jet A fuel and compared with the diesel control test fuel (DF-2). Fuel characteristics for both are shown in table V. The cetane value for this particular batch of Jet A fuel is essentially the same as DF-2 (47.3 and 47.8, respectively). The cetane value for Jet A, however, is not normally controlled at the refinery and can have a wider range of values. Aromatics and olefins, however, are about 50 percent lower for Jet A. Comparative emissions characterization results for both fuels are shown in figure 47 for 2000 and 2500 rpm. Tests were conducted at three fuel settings, 100, 120, and 140 mm^3 per cycle. The same injection timing was used for both fuels, and no attempt was made to optimize injection timing for Jet A fuel. At both 2000 and 2500 rpm lower peak cylinder gas pressure and lower BSNOX resulted with Jet A fuel, but higher BSHC emissions resulted. At 2500 rpm BSFC, BSCO, and particulate mass emissions were lower with Jet A fuel. But at 2000 rpm the values were lower with DF-2 fuel.

Friction Mean Effective Pressure/Power

Motored friction is normally used as a convenient way to calculate IMEP by adding the motored friction mean effective pressure (MEP) to the measured brake MEP, as determined from the dynamometer output. Motored friction MEP, which includes the pumping loop MEP for four-stroke cycle engines, does not account for actual firing pressures and temperatures, thermodynamic environment, and gas flow dynamics. The importance of these considerations is more apparent with supercharged and turbocharged engines. Now, with the convenience of sophisticated electronic chips and microprocessors, various schemes are available for real-time displays of engine parameters. The Lewis developed MEIS (ref. 2) provides a real-time computation of the total indicated mean effective pressure ($IMEP_t$) from the pressure-volume diagram. It is the sum of the compression-expansion and intake-exhaust loop MEP's. The MEIS was modified to provide, independently, the $IMEP_u$ value of the compression-expansion loop (upper loop of the diagram), the PMEP value of the intake-exhaust or pumping loop (lower loop of the diagram), and the sum of the upper loop + the lower loop of the pressure-volume diagram ($IMEP_t$). Actual FMEP values under loaded engine conditions can now be assessed on a real-time basis on four-stroke-cycle engines to provide more accurate engine results. The FMEP is equal to ($IMEP_u$ + PMEP) – BMEP. The $IMEP_u$ is shown in figure 48 to be a constant value across the engine speed range with the engine under load for each of three fuel quantities, while maintaining a constant inlet air pressure of 260 kPa and a constant exhaust backpressure of 210 kPa. The sum $IMEP_u$ + PMEP for the same set of conditions shows the negative influence of pumping work, or pumping mean effective pressure, with increased speed. Values of $IMEP_u$ + PMEP greater than the $IMEP_u$ value at 1500 rpm demonstrate the potential of a positive pumping loop, as with pressure compounding. BMEP decreases because of increasing pumping and friction losses with increasing speed. Figure 49 shows the actual values of FMEP for each of three fuel quantities under hot firing conditions. These values are derived from the MEIS outputs for the $IMEP_u$

12

and PMEP, and from dynamometer output for BMEP. The FMEP in this context does not include PMEP but does include all other mechanical losses.

In figure 50 friction MEP for an engine under load is compared with a motored engine for a naturally aspirated environment. Both sets of data are plotted for friction values as determined from MEIS computation, where

$$FMEP = (IMEP_u + PMEP) - BMEP.$$

This comparison demonstrates the increase in friction MEP with an engine under load, compared with one that is motored under no-load conditions. As shown in figure 51, FMEP values determined from motoring the engine are only slightly sensitive to inlet boost conditions. The change in the slope of the line for naturally aspirated conditions is attributable to the change in inlet-to-exhaust pressure ratio. Figure 52 demonstrates the influence of load (increase in fuel quantity) on FMEP, and values are compared with two motoring friction conditions operating under different inlet boost conditions. Real-time values of actual FMEP were 19 to 29 percent higher for the engine under load than for a motored engine.

Figure 53 shows actual friction power values computed from a motored engine at three inlet air pressures. Figure 54 compares the motored friction power value with values calculated from an engine operating under three loads to demonstrate the increase in actual friction loss with an engine under load. In conventional practice, however, motored friction values include the pumping losses. Figure 55, therefore, shows the equivalent values from the MEIS instrumentation for a motored engine by adding the pumping power values to the friction power values at three inlet air pressures. These values are equivalent to those obtained by the conventional procedure of motoring the engine and show the influence of inlet air pressure on power loss across the speed range.

Pumping Mean Effective Pressure/power

With the MEIS instrumentation, it is also practical to quantify the difference in pumping work from a motored engine under different operating conditions and to compare these values with those of an engine operating under load. Figure 56 compares the PMEP values from a motored engine under three inlet air pressure conditions and two inlet-to-exhaust pressure ratios. Pumping power values for the same conditions are shown in figure 57 and demonstrate the increasing power loss due to increases in inlet air pressure. A comparison is made with an engine under load in figure 58. PMEP values from an engine under load are shown to be lower than those of a motoring engine and insensitive to increased load, or fuel quantity, at any particular speed.

Figure 59 is a composite plot showing the combined total of FMEP and PMEP for a motored engine at three inlet air pressures and for an engine operated at three loads and 262 kPa (38 psia) inlet air pressure. For the same inlet and exhaust pressures, the values of FMEP + PMEP from a motored engine were higher than for an engine under load at all speeds, except 3000 rpm where the two lines converge at higher load conditions (140 mm^3/cycle).

Pressure Compounding

The concept of pressure compounding is intended to transform the negative work, normally contained in the pumping loop of the four-stroke thermodynamic cycle, to a

13

positive value. This can be accomplished by adjusting the magnitude of inlet-air and exhaust-gas pressures. Figure 60 shows enlargements of the pumping loop diagrams for the engine operating at an inlet pressure of 262 kPa and three exhaust back pressures and at 2000 rpm. Figure 61 shows pumping loop diagrams for the engine running at the same speed but with an inlet pressure of 413 kPa. The summary of these data (table VII) indicates that significant reductions in pumping losses can be accomplished with higher pressure ratios (PI/PE) across the cylinder. Positive work output from the pumping loop can be accomplished by increasing the inlet air pressure, by decreasing the exhaust back-pressure, or by a combination of both methods. For this example, a 13 percent reduction in BSFC is obtained by increasing the inlet air pressure by a factor of 1.6 and by reducing the exhaust back pressure by 40 percent.

Figure 62 is a plot of $IMEP_u$ and $IMEP_u$ + PMEP versus exhaust backpressure for two speeds, 2000 and 2500 rpm, and four fuel quantities: 80, 100, 120 and 140 mm^3/cycle. For 262 kPa inlet pressure, zero pumping load occurs at an exhaust backpressure of 154 kPa for 2500 rpm and at 185 kPa for 2000 rpm, regardless of the fuel injected quantity or engine load. The $IMEP_u$ is shown to be essentially constant at each load and speed setting regardless of the pressure ratio (PI/PE) value. The pressure ratio, however, does influence BMEP values as shown in figure 63. The point of transition between positive and negative pumping loop values occurs at a pressure ratio of 1.4 for 2000 rpm and at 1.7 for 2500 rpm. Figure 63 also shows the net gain in power, or BMEP, at four fuel quantities for pressure ratios greater than 1.4 and 1.7 for 2000 and 2500 rpm, respectively. A 1.25 pressure ratio was used throughout this project to simulate back-pressure from a conventional turbocharger. The percent increase in BMEP, by increasing the pressure ratio from 1.25 to 2.62 maximum, is shown in table VIII to be in the range of 3.4 to 6.7 percent improvement.

Pressure compounding is shown to provide the opportunity of improving overall engine performance by controlling the inlet boost pressure and reducing exhaust backpressure. One method that can be effectively used on turbocharged engines is a "blow-down" turbine where each cylinder discharges independently to separate turbine nozzles and then discharges to atmosphere.

Encoder Misalignment Effects

Figure 64 shows the effect on IMEP readings with the modular engine instrumentation system (MEIS) if the encoder zero crank angle signal is not set at exactly top dead center of the cylinder. These plots demonstrate the importance of precision when setting up the encoder. The error can be greater than 11 percent for a 1° misalignment. The encoder signal was displaced electronically for this demonstration.

CONCLUSIONS

Inlet Pressure Effects

1. Optimum engine performance (BSFC and BMEP) occurs at approximately 329-kPa inlet air pressure when the cylinder pressure ratio is maintained at 1.25, representative of backpressure from a typical state-of-the-art turbocharger system.

2. Peak cylinder gas temperature is an inverse function of inlet air mass and proportional to load or fuel quantity per cycle.

Inlet Temperature Effects

3. Volumetric efficiency is a misleading parameter for supercharged engines. BMEP and BSFC are more meaningful indicators of engine performance at different inlet air temperatures.

4. Optimum injection timing for BSFC and BMEP is not influenced by inlet air temperature.

Exhaust Emissions

5. Calculated values for total particulate mass, based on exhaust smoke opacity, correlate best with the solid fraction of the total measured particulate matter. The soluble organic fraction of the total measured particulate correlates more closely with the hydrocarbon emission measurement than with smoke opacity.

6. Both total particulate matter and hydrocarbon emissions decrease with increased load between 1500 and 3000 rpm.

7. The lowest levels of exhaust smoke and gaseous emissions occur with inlet air pressures greater than 372 kPa, while maintaining the pressure ratio at 1.25.

8. Operation at 2500 and 2000 rpm with Jet A fuel resulted in lower oxides of nitrogen emissions and peak cylinder gas pressures, but higher hydrocarbon emissions, than those obtained with DF-2. At 2500 rpm, BSFC, BSCO, and total particulate mass emissions were lower with Jet A fuel, but at 2000 rpm, these emissions were lower with DF-2 fuel.

Modular Engine Instrumentation System (MEIS)

9. Use of MEIS instrumentation requires accurate precision when timing the shaft angle encoder signal to the engine for top dead center location. Errors greater than 11 percent of net IMEP can result with 1° crank angle misalignment.

10. MEIS instrumentation provides a more accurate and convenient method for real-time measurement of friction power than by the conventional motoring method.

11. Positive work output from the pumping loop can be obtained either by increasing the inlet air pressure, by decreasing the exhaust backpressure, or by a combination of both methods. A 13-percent improvement in BSFC was shown by increasing the pressure ratio from 1.25 to 3.33 at 2000 rpm.

REFERENCES

1. Funkenbusch, E.F.; Leddy, D.G.; and Johnson, J.H.: The Characterization of the Soluble Organic Fraction of Diesel Particulate Matter. SAE Paper 790418, Feb. 1979.

2. Rice, W.J.; and Birchenough, A.G.: Modular Instrumentation System for Real-Time Measurements and Control on Reciprocating Engines. NASA TP-1757, 1980.

3. Taylor, Charles F.: The Internal-Combustion Engine in Theory and Practice, Vol. II: Combustion, Fuels, Materials, Design, MIT Press, 1968.

4. A Laboratory Comparison of In-Line and End-of-Line Full-Flow, Diesel Smoke Opacity Meters. CRC-APRAC-CAPI-1-64, Coordinating Research Council, Inc., 1977, (PB-278 076).

5. Vuk, C.T.; Jones, M.A.; and Johnson, J.H.: The Measurement and Analysis of the Physical Character of Diesel Particulate Emissions. SAE Paper 760131, Feb. 1976.

6. Greeves, G.; and Wang, C.H.T.: Origins of Diesel Particulate Mass Emissions. SAE Paper 810260, July 1981.

TABLE I. - EXHAUST GAS ANALYSIS INSTRUMENTS

Constituent	Type of instrument	Measurement range
CO	Nondispercive infra-red	0 to 2500 ppm, 0 to 10 percent; 3 ranges
CO_2	Nondispercive infra-red	0 to 15 percent; 3 ranges
NO/NO_x	Heated chemiluminescence	0 to 10 000 ppm; 9 ranges
HC	Heated flame ionization	0 to 10 000 ppm; 8 ranges
O_2	Paramagnetic	0 to 25 percent; 4 ranges

TABLE II. - SPAN GAS BOTTLES

Span gas	Concentration
C_3H_8 in air	14.8 ppm 29.6 ppm 152 ppm 304 ppm
O_2 in N_2	8 percent
CO_2 in O_2 Free N_2	2.42 percent 3.96 percent 13 percent
NO in N_2	1197 ppm 1 percent 4.05 percent
NO in N_2	36.5 ppm 455 ppm 820 ppm 4090 ppm

TABLE III. - SPECIFICATION AND OPERATING GUIDELINES FOR

PARTICULATE MEASUREMENT

```
Standard conditions
  Temperature, °C (°F) . . . . . . . . . . . . . . . . . . . . . . . . . . . 20 (68)
  Pressure, kPa (in. of Hg) . . . . . . . . . . . . . . . . . . . . 101.3 (29.92)
Filter size, mm diam . . . . . . . . . . . . . . . . . . . . . . . . . . . . . 47
Pump displacement per revolution, m³ (ft³) . . . . . . . . . . . . 0.017 (0.6)
Probe flow rate (maximum), liter/s (scfm) . . . . . . . . . . . . . 0.47 (1.0)
Filter flow rate (minimum), liter/s (scfm) . . . . . . . . . . . . . 9.8 (0.35)
Probe temperature (maximum), °C (°F) . . . . . . . . . . . . . . . . 52 (125)
Filter loading, mg . . . . . . . . . . . . . . . . . . . . . . . . . . . . 2 to 7
```

TABLE IV. - MAJOR MEASURED PARAMETERS

Parameter	Instrument	Full scale value
Fuel flow	Hydraulic wheatstone bridge mass flowmeter	0.037 kg/s (tp lb m/hr)
Engine airflow	Turbine type flowmeter	47 liter/s (100 scfm)
Engine torque	Load cell on the dynamometer	347 J (256 ft-lb)
Engine speed	Magnetic pick-up	6144 rpm
Cylinder pressure	Water-cooled piezoelectric quartz transducer	27.6 MPa (4000 psig)
Injection pressure	Strain gage transducer	69 MPa (10 000 psig)
Engine inlet air pressure	Strain gage transducer	765 kPa (111 psia)
Engine inlet air temperature	Chromel alumel thermocouple	121° C (250° F)
Blow by	Displacement type flowmeter	8.5×10^{-4} m³/s (1.8 scfm)
Engine exhaust pressure	Strain gage transducer	690 kPa (100 psia)
Engine exhaust temperature	Chromel alumel thermocouple	1024° C (1876° F)

TABLE V. - BASELINE EMISSIONS
[Injection timing set for optimum performance]

Fuel quantity mm^3/cycle	Number of tests	Brake mean effective pressure, BMEP, kPa (psi)	Air to fuel ratio	Brake specific emission, g/kW-hr (standard deviation)					Soluble organic fraction, SOF, percent
				CO	HC	NO$_x$	Particulates		
							Measured	Calculated	
Engine speed, 1500 rpm									
60	5	612 (89)	79.5	3.67 (0.30)	2.71 (0.29)	15.78 (0.12)	1.33 (0.39)	0.40	49.4
80	6	869 (126)	58.9	2.25 (.36)	1.89 (.17)	18.41 (.15)	1.11 (.46)	.23	63.3
100	7	1124 (163)	47.2	1.65 (.12)	1.37 (.07)	20.48 (.76)	0.75 (.07)	.27	62.8
120	6	1350 (196)	39.3	1.92 (.21)	1.17 (.04)	19.86 (.44)	.78 (.05)	.43	37.1
140	6	1551 (225)	33.8	2.31 (.19)	0.95 (.03)	18.36 (.72)	.75 (.04)	.63	----
Engine speed, 2000 rpm									
60	8	521 (76)	74.2	4.65 (0.15)	2.97 (0.47)	15.76 (0.68)	1.77 (0.36)	0.44	75.3
80	10	785 (114)	54.9	2.45 (.24)	1.92 (.16)	15.73 (.37)	0.99 (.28)	.25	74.1
100	10	1027 (149)	43.8	1.81 (.24)	1.64 (.16)	17.63 (.27)	.96 (.19)	.30	76.9
120	10	1267 (184)	36.4	2.14 (.46)	1.26 (.11)	18.88 (.87)	.78 (.27)	.40	52.4
140	9	1437 (208)	30.8	3.85 (.16)	1.23 (.05)	18.40 (.27)	1.26 (.03)	1.02	----
Engine speed, 2500 rpm									
60	10	418 (61)	64.7	6.19 (0.86)	3.58 (0.42)	21.25 (1.26)	2.52 (0.66)	0.46	78.0
80	7	692 (100)	49.6	3.08 (.91)	2.13 (.34)	17.55 (.56)	1.58 (.66)	.37	78.7
100	13	968 (140)	39.3	2.61 (.70)	1.65 (.31)	17.93 (.46)	1.11 (.36)	.43	60.5
120	11	1184 (172)	33.1	3.60 (1.26)	1.39 (.17)	18.34 (.51)	0.94 (.11)	.35	56.3
140	6	1374 (199)	27.9	4.65 (.31)	1.18 (.16)	16.94 (2.61)	0.91 (.04)	.62	----
Engine speed, 3000 rpm									
60	4	355 (51)	63.9	7.30 (0.79)	4.65 (0.54)	20.29 (0.78)	2.05 (0.50)	0.81	80.1
80	6	590 (86)	46.5	4.25 (.50)	2.52 (.25)	16.60 (.80)	1.33 (.35)	.52	58.9
100	6	830 (120)	38.0	3.39 (.06)	1.84 (.05)	15.25 (.29)	1.19 (.13)	.68	37.2
120	7	1057 (153)	32.3	3.83 (0.72)	1.47 (.15)	14.54 (.40)	0.91 (.05)	.68	25.2
140	6	1287 (187)	27.3	5.64 (0.23)	1.03 (.05)	15.50 (1.61)	0.94 (.04)	.78	----

TABLE VI. - DIESEL AND JET A FUEL CHARACTERISTICS

Property	(ASTM) test method	Diesel control fuel	Jet A
Gravity, °API	D-287	34.696	42.58
Specific gravity	D-1290	0.8514	0.8128
Heat content of fuel:			
Gross, MJ/kg (Btu/lb)	D-240	45 (19 228)	45.5 (19 561)
Gross, MJ/m^3 (Btu/gal)	D-240	37 976 (136 375)	36 880 (132 438)
Net, MJ/kg (Btu/lb)	Calculation	42.0 (18 043)	42.6 (18 312)
Hydrogen to carbon ratio	Calculation	1.777	1.905
Hydrogen, wt %	Chromatography	12.98	13.69
Carbon, wt %	Chromatography	86.85	86.25
Sulfur, wt %	D-129	0.31	0.063
Cetane index	D-976	47.8	47.3
Aromatics, vol %	D-1319	29.61	15.21
Olefins, vol %	D-1319	1.40	0.78
Saturates, %	D-1319	68.99	84.08
Distillation, °C (°F)			
Initial boiling point, °C (°F)	D-86	191 (376)	160 (320)
10%,	D-86	219 (426)	184 (364)
50%,	D-86	264 (508)	214 (418)
90%,	D-86	302 (576)	251 (484)
End point,	D-86	315 (599)	273 (524)
Kinematic viscosity, C S (m2/s)	D-445	3.67	2.0
Flash point, °C (°F)	D-93	73 (163)	49 (120)
Cloud point, °C (°F)	D-2500	-19 (-2)	-20.6 (-5)
Pour point, °C (°F)	D-97	-41 (-42)	-51.7 (-61)
Aniline point, °C (°F)	D-611	60 (140)	62 (144)

TABLE VII. - PRESSURE COMPOUNDING RESULTS AT 2000 RPM

[Engine speed, 120 mm^3/cycle]

Inlet air pressure, kPa (psia)	Exhaust pressure, kPa (psia)	Pressure ratio	Mean effective pressures, kPa (psia)			Brake specific fuel consumption, BSFC, kg/kW-hr
			Indicated, $IMEP_u$	Pumping, PMEP	$IMEP_u$ + PMEP	
262 (38)	210 (30)	1.25	1588 (230)	-37 (-5.5)	1551 (225)	0.217
262 (38)	152 (22)	1.72	1588 (230)	+25.5 (+3.7)	1613 (234)	.208
262 (38)	110 (16)	2.40	1578 (229)	+67 (+9.7)	1645 (239)	.202
414 (60)	331 (48)	1.25	1613 (234)	-41.4 (-6)	1572 (228)	.213
414 (60)	207 (30)	2.00	1620 (235)	+76 (+11)	1696 (246)	.195
414 (60)	124 (18)	3.33	1613 (234)	+138 (+20)	1751 (254)	.188

TABLE VIII. - MEAN EFFECTIVE PRESSURE AT TWO
PRESSURE RATIOS

Engine speed, rpm	Fuel quantity, mm3/cycle	Pressure ratio		Increase in BMEP, percent
		1.25	2.62	
		Brake mean effective pressure, BMEP, kPa (psi)		
2000	80	----------	----------	---
	100	1065 (154)	1135 (164)	6.6
	120	1300 (188)	1365 (198)	5.0
	140	1500 (217)	1580 (229)	5.3
2500	80	750 (109)	800 (116)	6.7
	100	1020 (148)	1070 (155)	4.9
	120	1265 (183)	1315 (191)	4.0
	140	1485 (215)	1535 (223)	3.4

(a)   C-79-486

(b)   C-77-3617
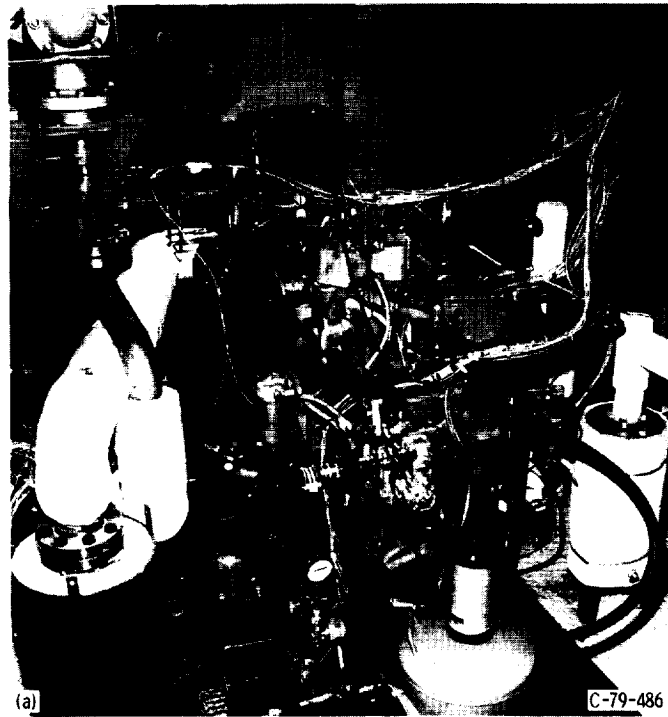
Figure 1. - Single-cyclinder test engine installation.
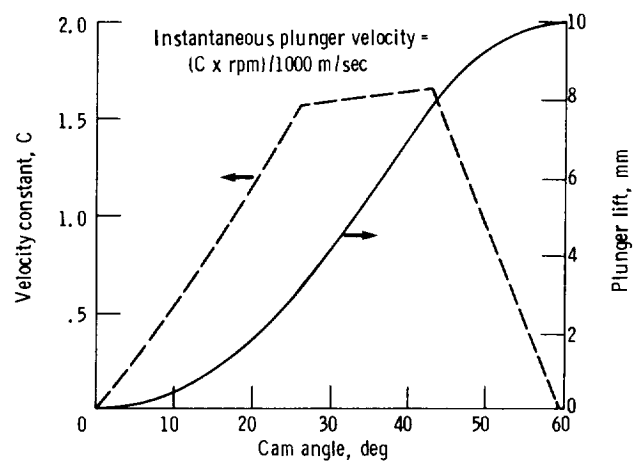
Figure 2. - Injection pump cam analysis.

(a) Data handling schematic.

Pressure regulator   Relief valve
Solonoid valve   Filter
Flow valve   Control valve
Flow meter   Gage
   Boost pump

(b) Flow schematic.
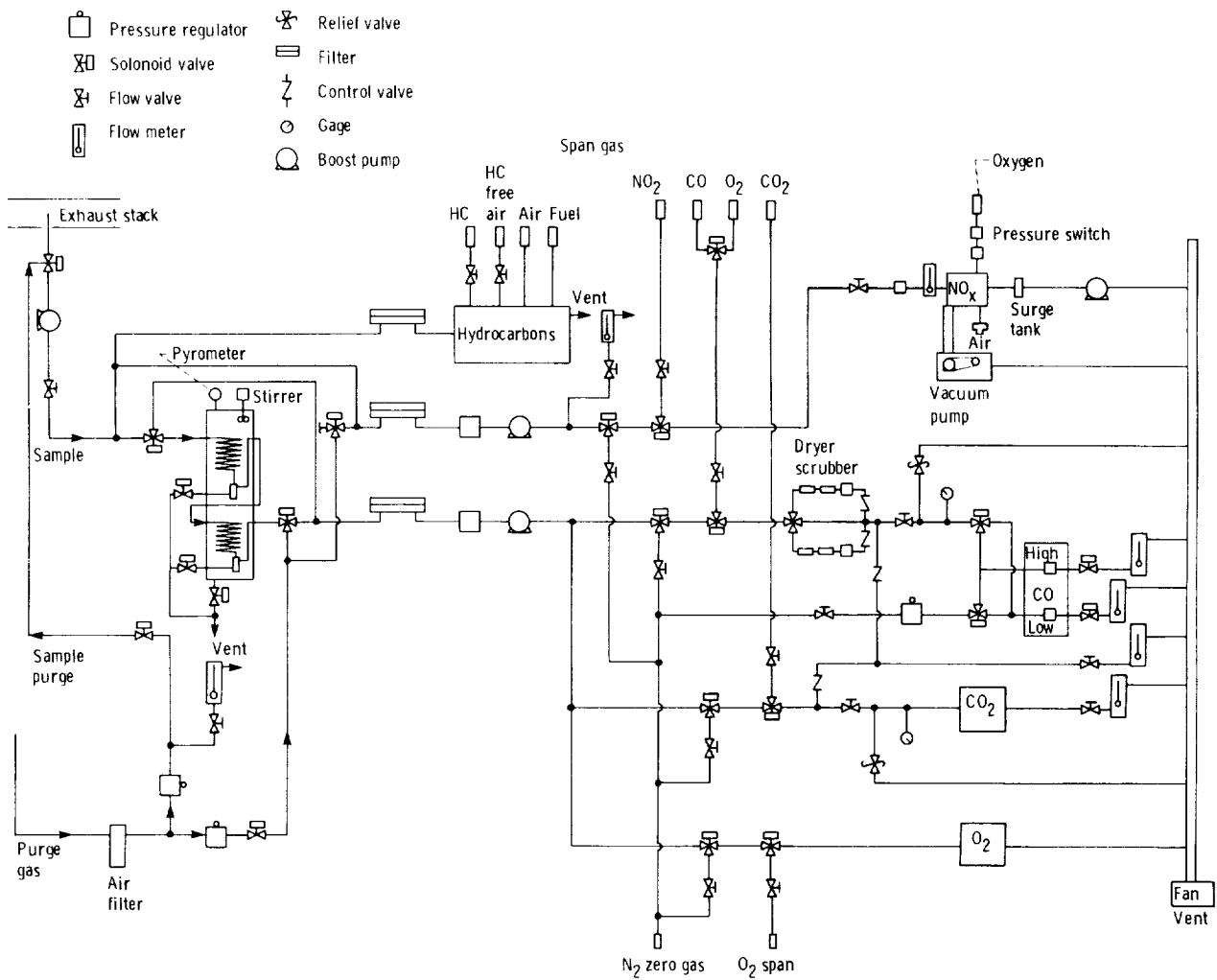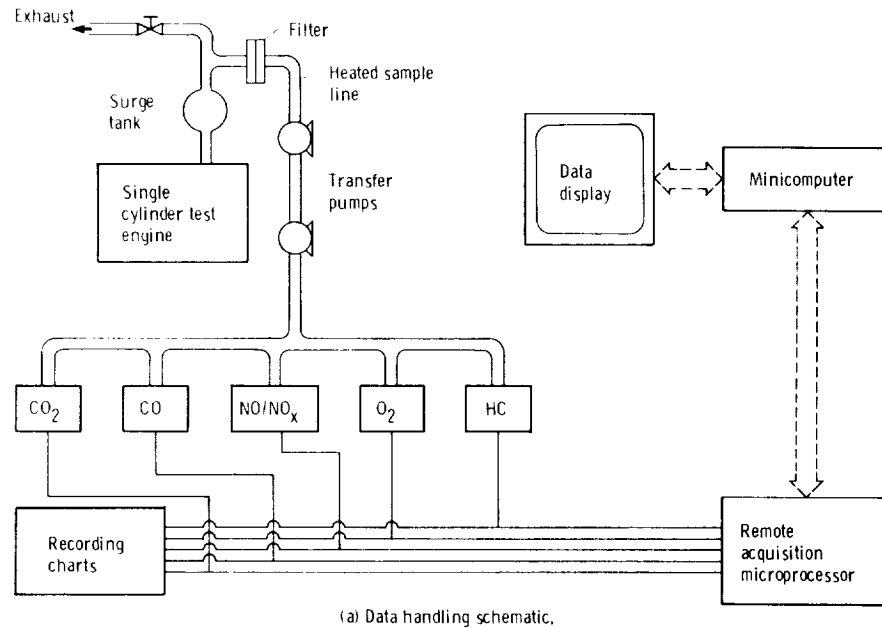
Figure 3. – Exhaust gas analysis system.

C-80-2276
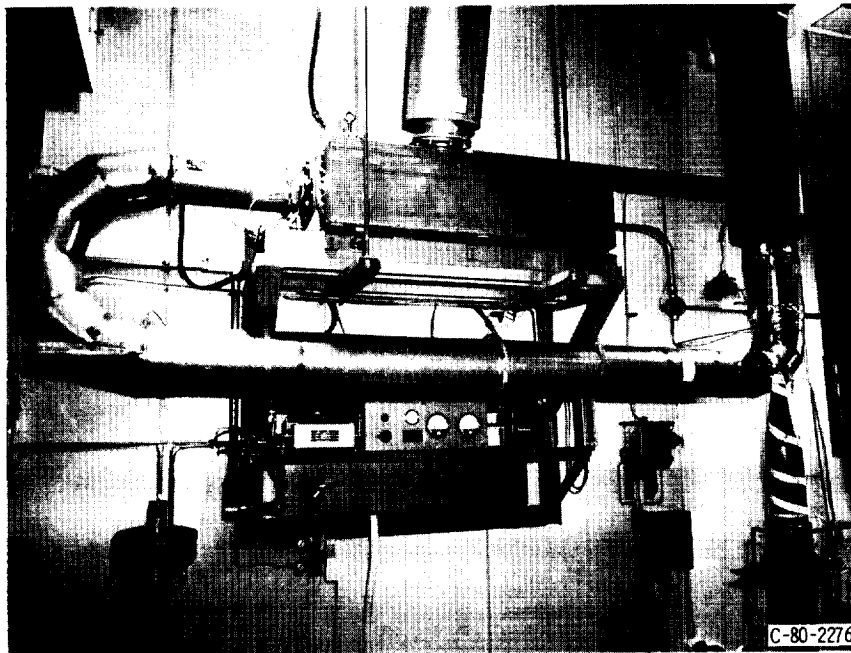
Figure 4. - Particulate sampling system.

(a)

C-79-486

Exhaust

Vent

Air supply

Electric heater 54° C

Inlet air

Max 520° C

Exhaust flow

Filter cassette

Sample probes

In-line opacity meter

By-pass filter

Engine exhaust

Surge tank

Vacuum pump

Muffler

Exhaust thru roof

Flowmeter CFM totalizer

In-line opacity meter

Dilute sample

To emissions analyzer -lines maintained 190° C
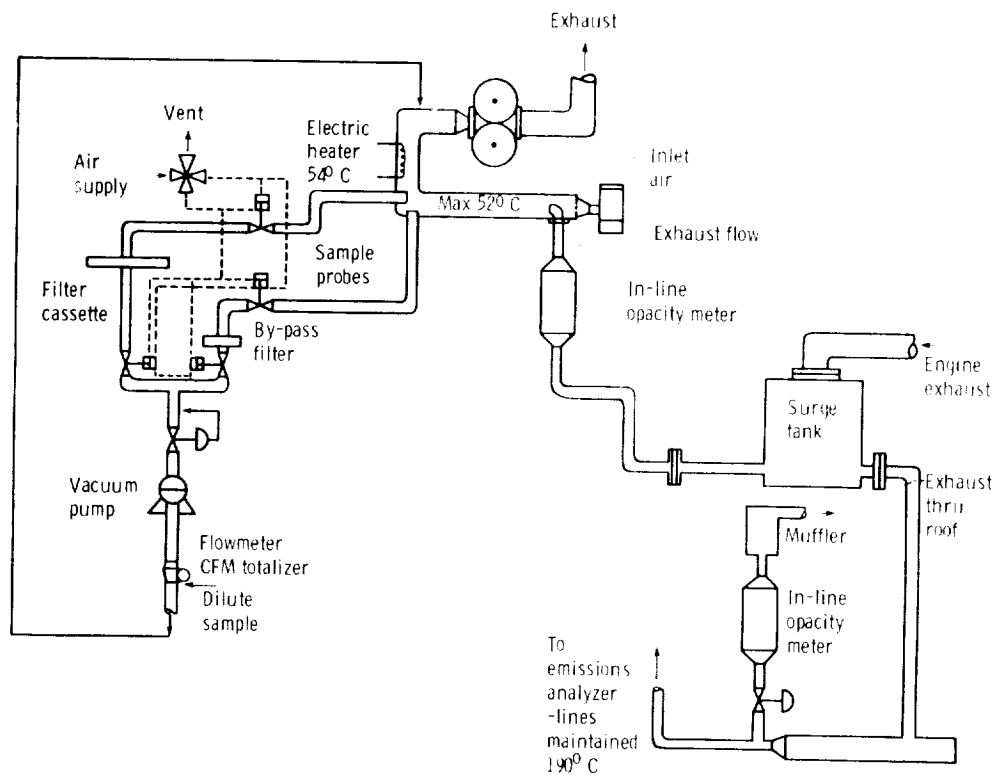
(b) Emission sampling system.

Figure 5. - Test operator console, instrument panel, and exhaust emissions console.
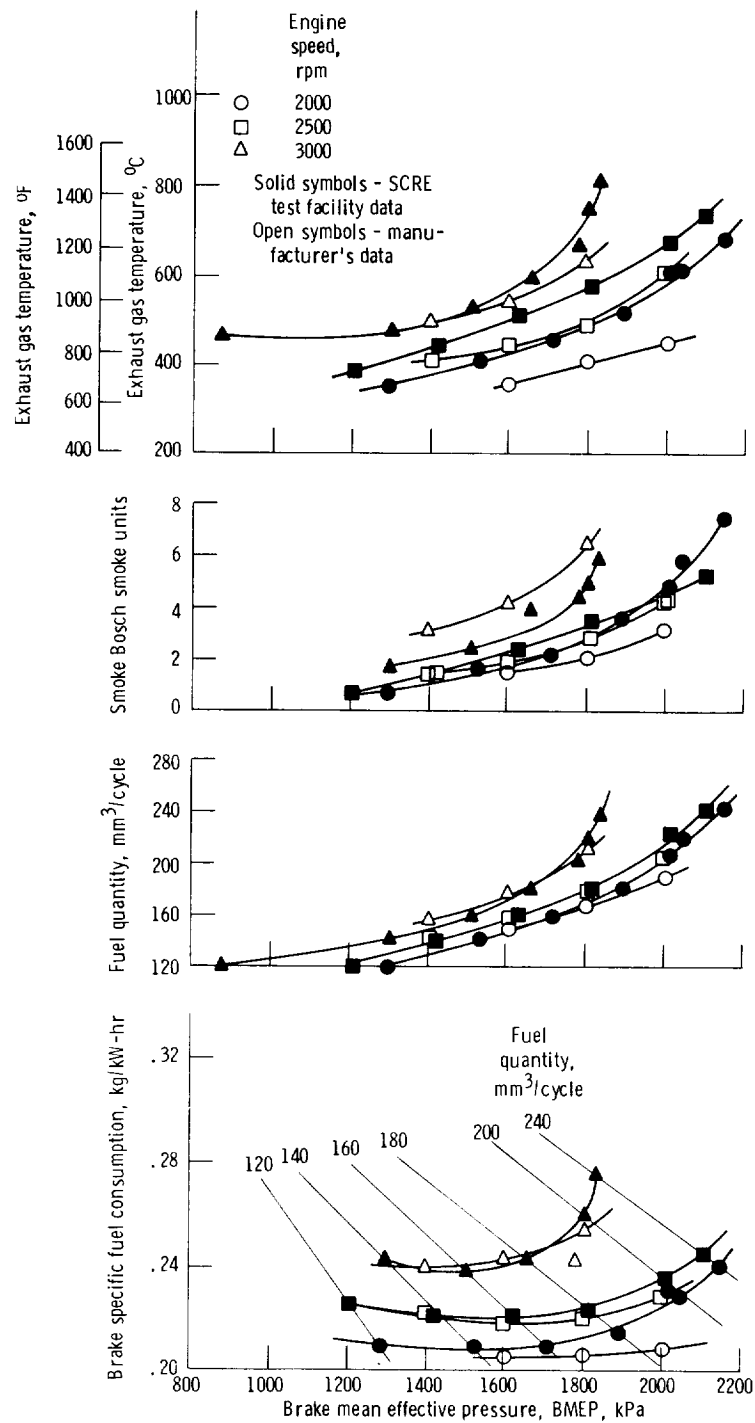
Figure 6. - NASA test data versus manufacturer supplied data.
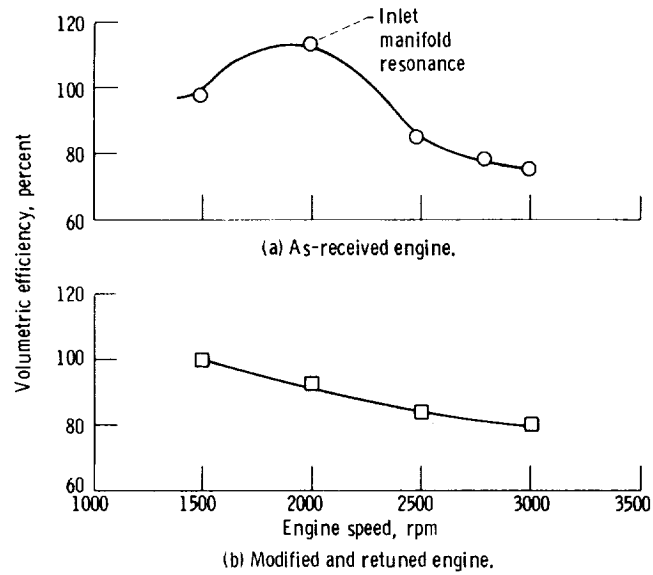
Figure 7. – Volumetric efficiency versus engine speed – effect of
inlet manifold pressure resonance.
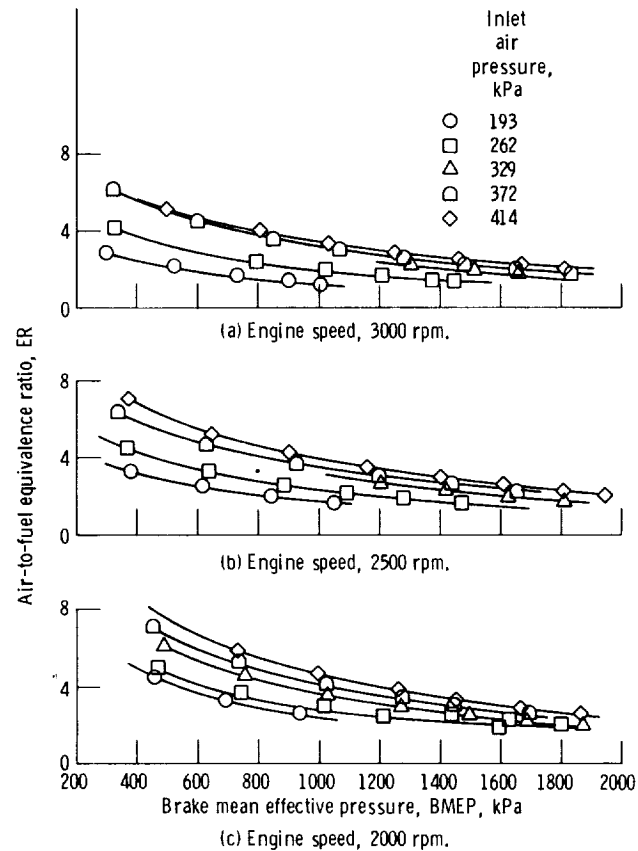
Figure 8. – Effect on air-to-fuel equivalence ratio with increasing
inlet air pressure at different BMEP's.
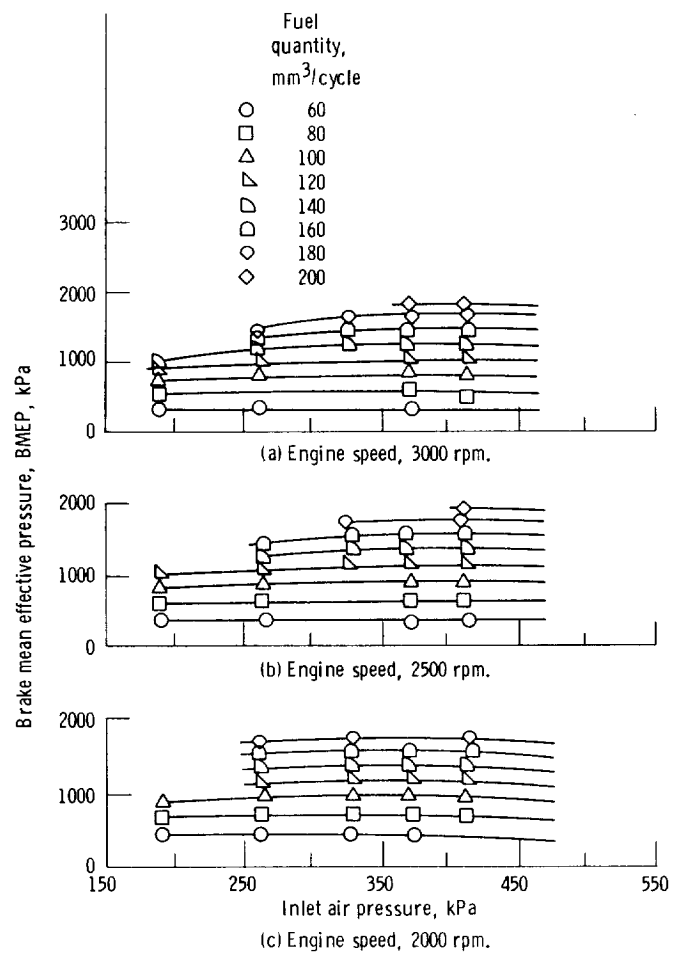
Figure 9. — Effect on BMEP with increasing inlet air pressure.
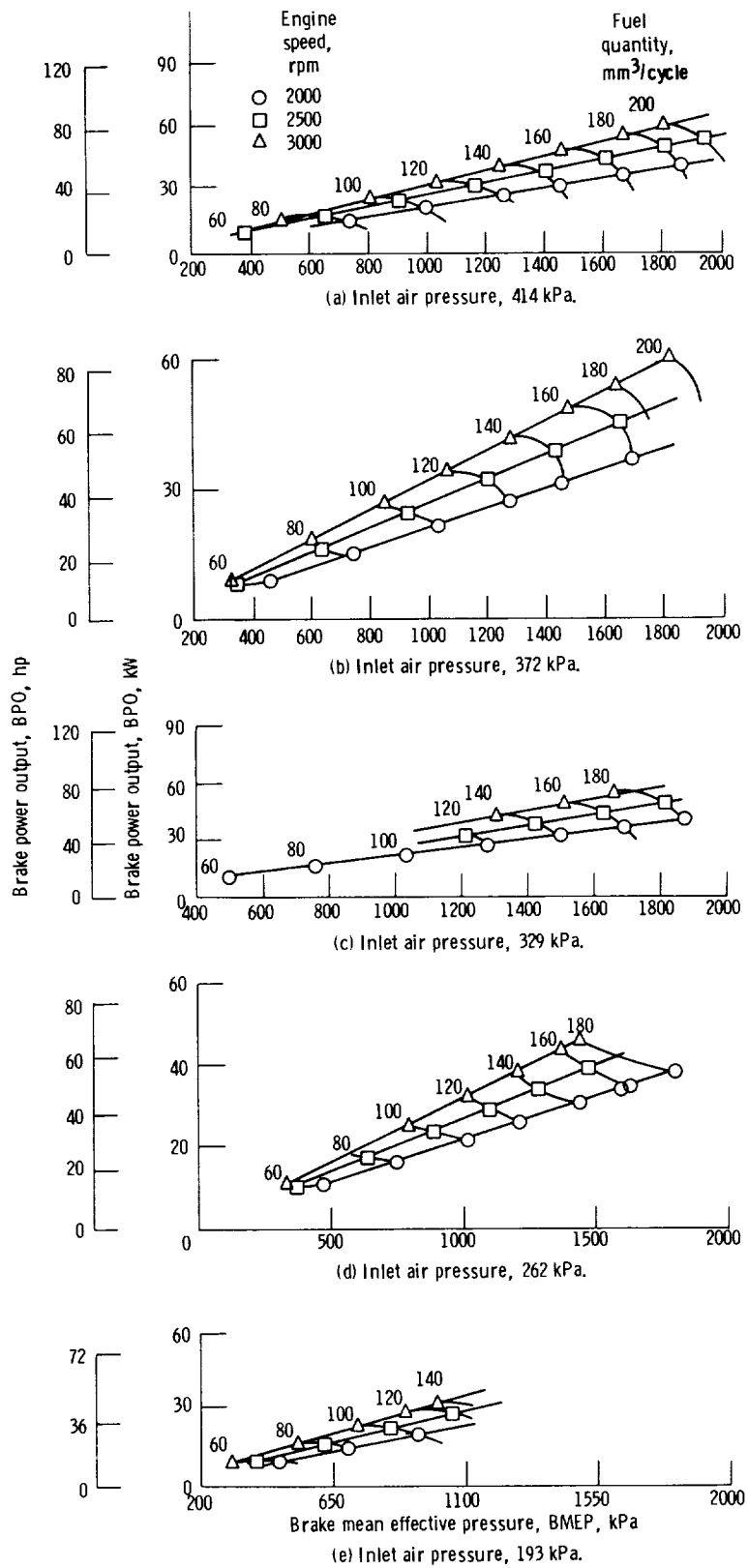
Figure 10. - Effect of engine speed on brake power output.
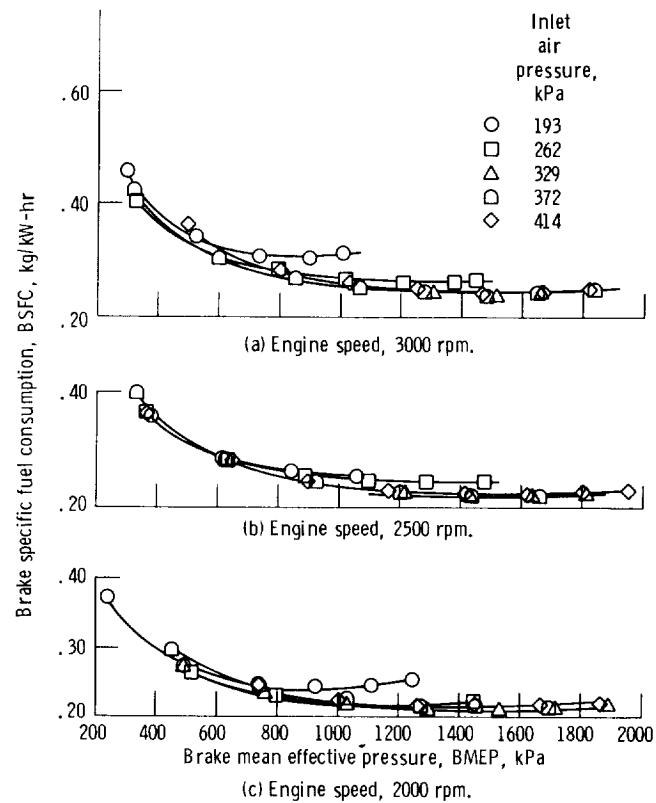
Figure 11. – Effect on BSFC with increasing inlet air pressure at different rpms.

(a) Engine speed, 3000 rpm.

(b) Engine speed, 2500 rpm.

(c) Engine speed, 2000 rpm.
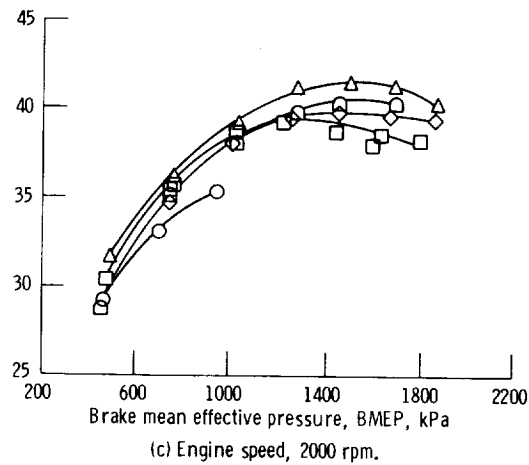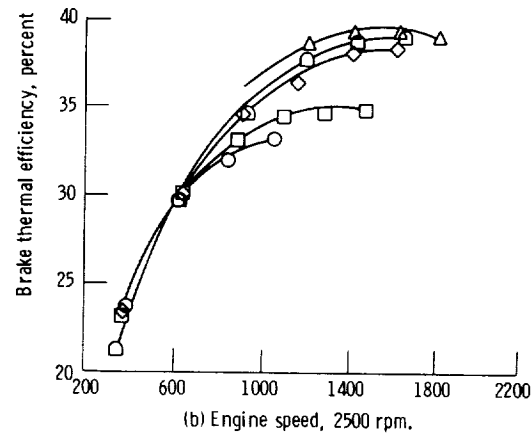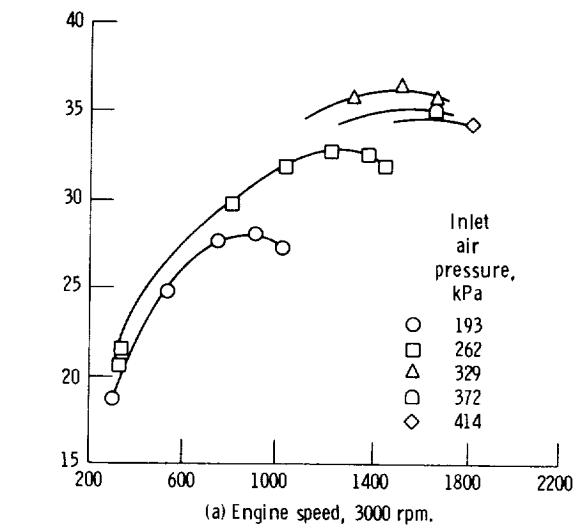
Figure 12. - Effect on brake thermal efficiency with increasing inlet air pressure at different rpms.
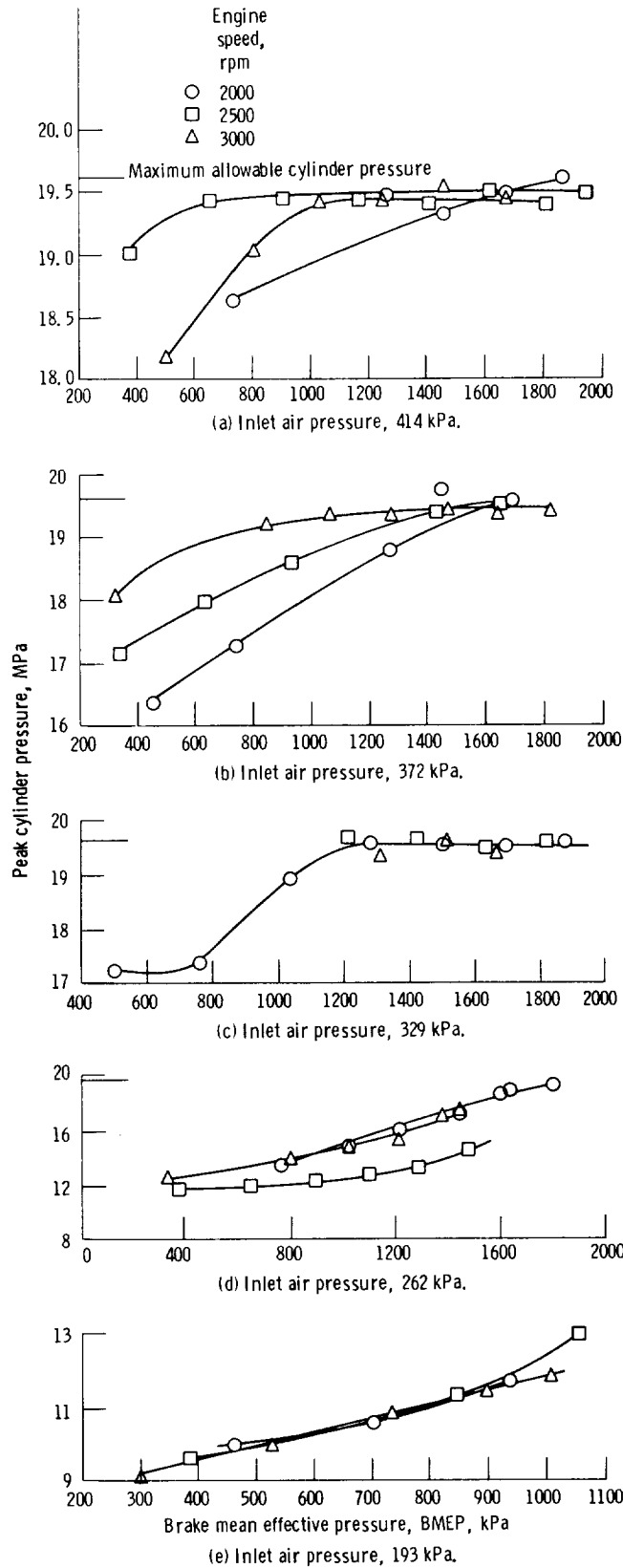
Figure 13. - Effect of engine speed on peak cylinder gas pressures at different inlet air pressures.
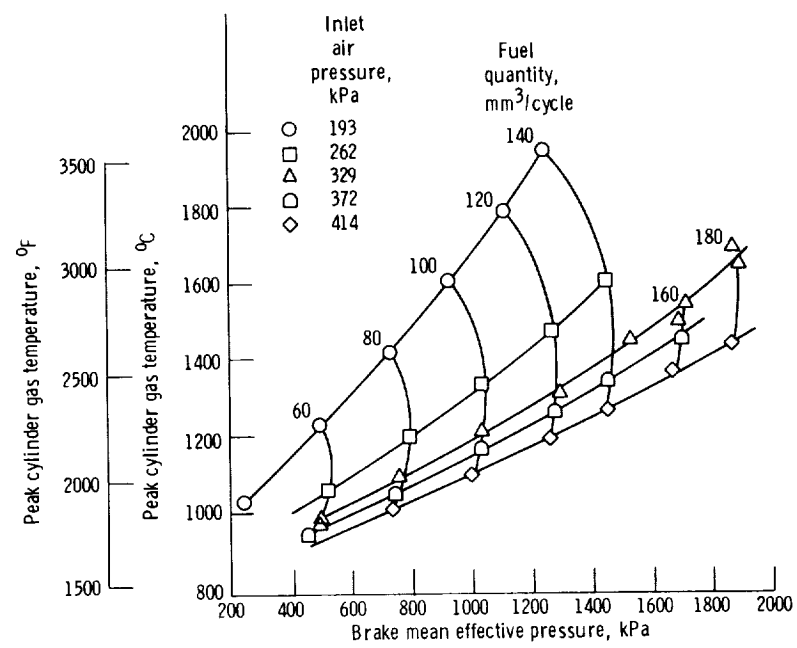
Figure 14. - Effect of inlet air pressure on peak cylinder gas temperature. Engine speed, 2000 rpm.
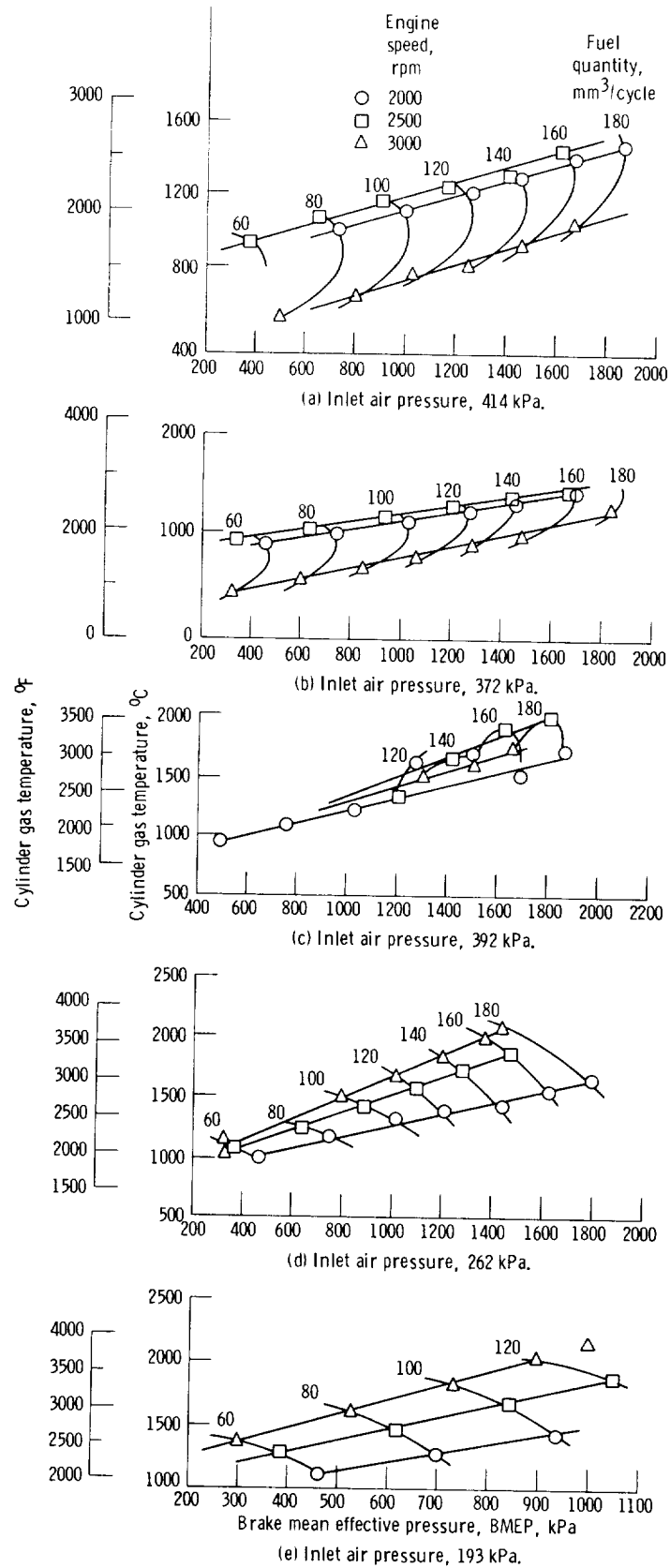
Figure 15. – Effect of engine speed on cylinder gas temperature.

Figure 17. - BMEP versus air-to-fuel ratio.

Figure 16. - Effect of inlet air pressure on engine exhaust temperature.

Figure 19 (top chart):

Inlet
air
pressure,
kPa

○ 193
□ 262
△ 329
◁ 372
◇ 414

Air-to-fuel ratio, A/F

Brake thermal efficiency, percent

45 40 35 30 25 20

20 40 60 80 100 120

Figure 19. – Brake thermal efficiency versus air to fuel ratio. Engine speed, 2000 rpm.

Figure 18 (bottom charts):

Inlet
air
pressure,
kPa

○ 193
□ 262
△ 329
◁ 372
◇ 414

(a) Engine speed, 3000 rpm.

(b) Engine speed, 2000 rpm.

Air-to-fuel ratio, A/F

Brake specific fuel consumption, BSFC, g/kW-hr

500 400 300 200

400 350 300 250 200

Figure 18. – BSFC versus air-to-fuel ratio at 2000 and 3000 rpm.
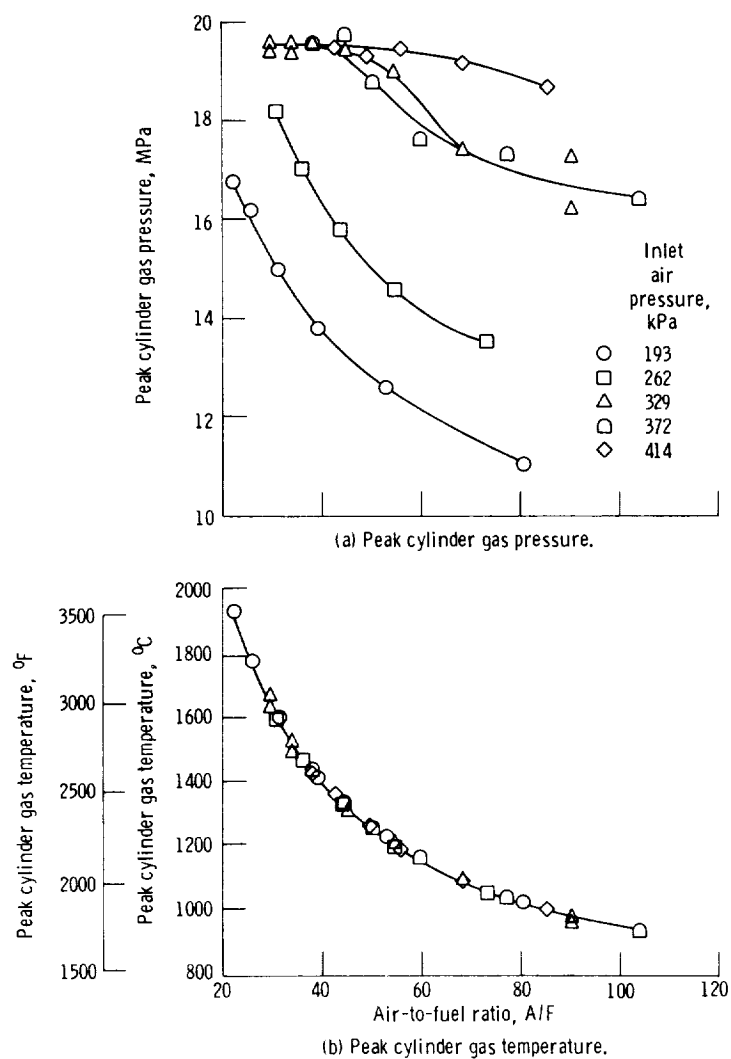
Figure 20. - Peak cylinder gas pressure and temperature versus air-to-fuel ratio. Engine speed, 2000 rpm.

(c) Engine speed, 2500 rpm; static timing, 40° BTDC.
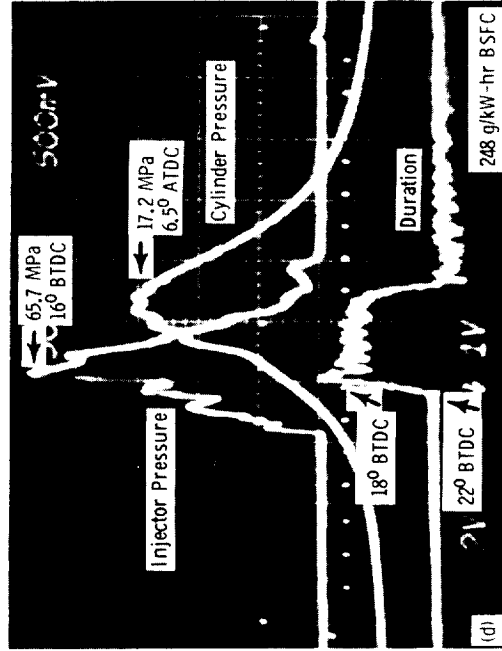
(d) Engine speed, 3000 rpm; static timing, 42° BTDC.

(a) Engine speed, 1500 rpm; static timing, 28° BTDC.

(b) Engine speed, 2000 rpm; static timing, 33.3° BTDC.

Figure 21. - Typical fuel injection and combustion gas pressure diagrams. Fuel quantity, mm³/cycle; inlet air pressure, 262 kPa.
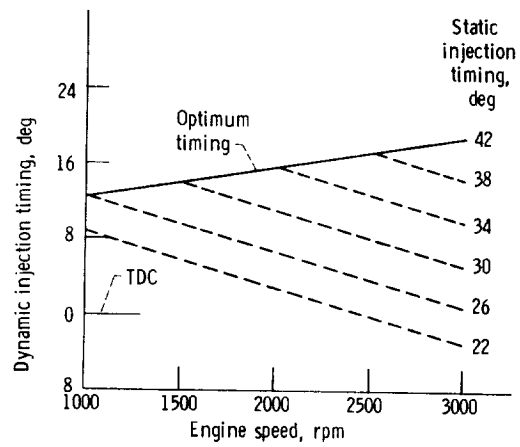
Figure 22. - Static versus dynamic injection
timing correlation.
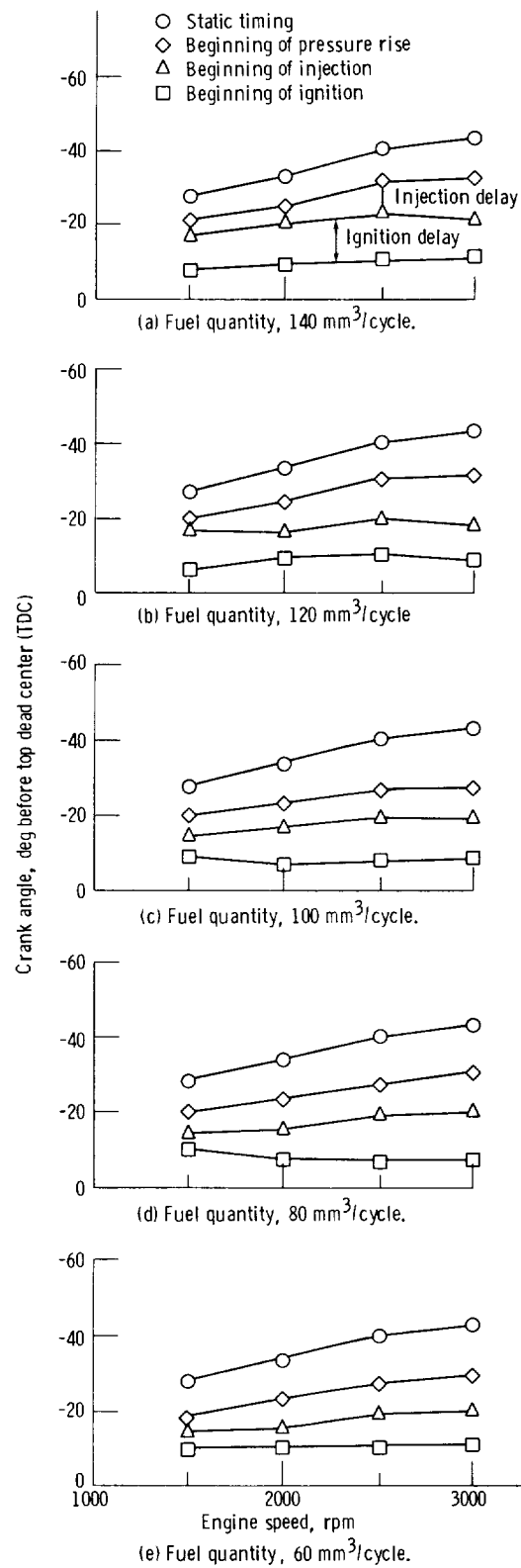
Figure 23. – Diesel fuel injection variables. Injection timing set for optimum performance.

Figure 25. – Effect of injection timing on BSFC. Inlet air temperature, 37.8° C; inlet air pressure, 262 kPa.

Fuel quantity, mm³/cycle
○ 60
□ 80
◁ 100
△ 120
◁ 140

(a) Engine speed, 2500 rpm.
(b) Engine speed, 2000 rpm.
(c) Engine speed, 1500 rpm.

Injection timing, deg before top dead center

Brake specific fuel consumption, BSFC, kg/kw-hr

Figure 24. – Effect of injection timing on BMEP. Inlet air temperature, 37.8° C; inlet air pressure, 262 kPa.

Fuel quantity, mm³/cycle
○ 60
□ 80
◁ 100
△ 120
◁ 140

(a) Engine speed, 2500 rpm.
(b) Engine speed, 2000 rpm.
(c) Engine speed, 1500 rpm.

Injection timing, deg before top dead center

Brake mean effective pressure, BMEP, kPa

Figure 26. - Inlet air mass as function of inlet
air temperature. Inlet air pressure, 262 kPa;
fuel quantity, 100 mm³/cycle.
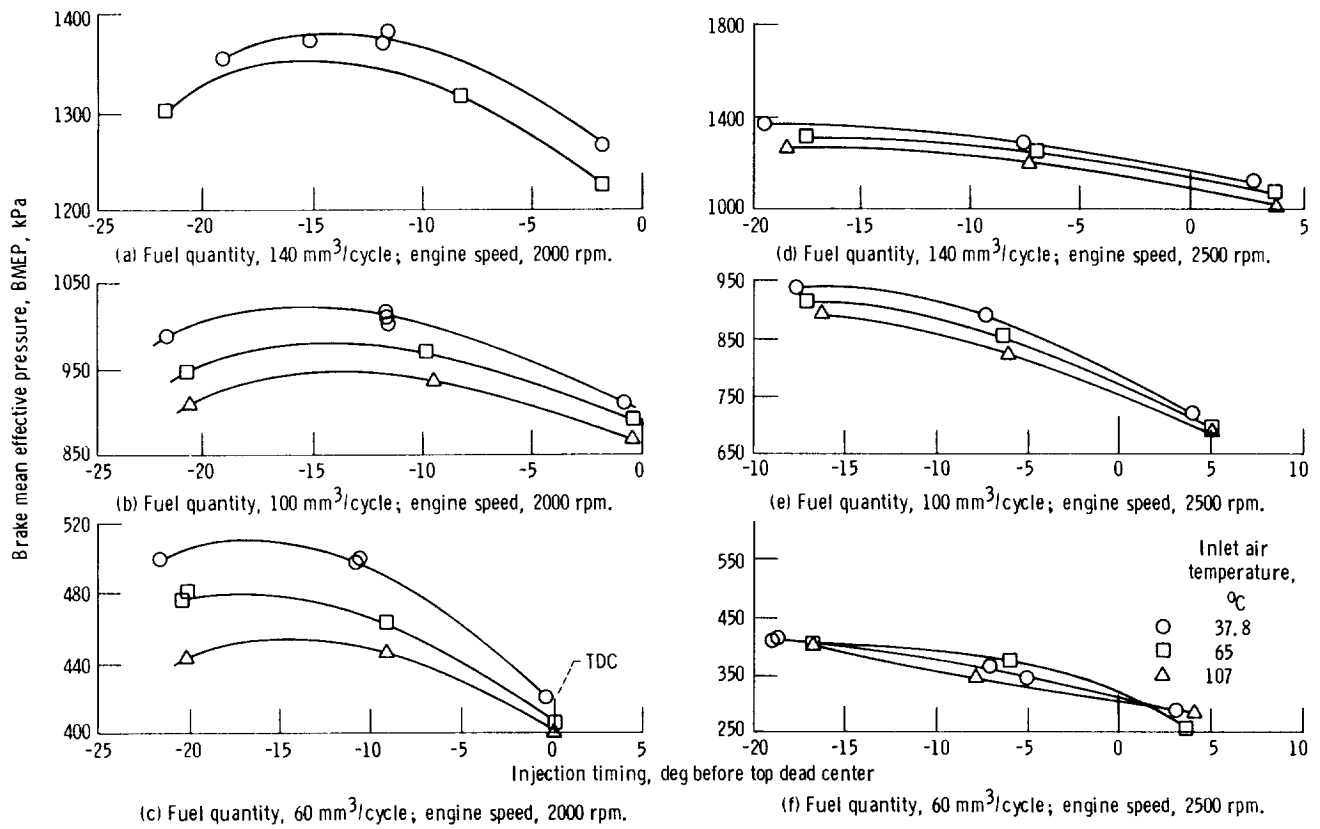
Figure 27. – Effect of inlet air temperature on BMEP. Inlet air pressure, 262 kPa.
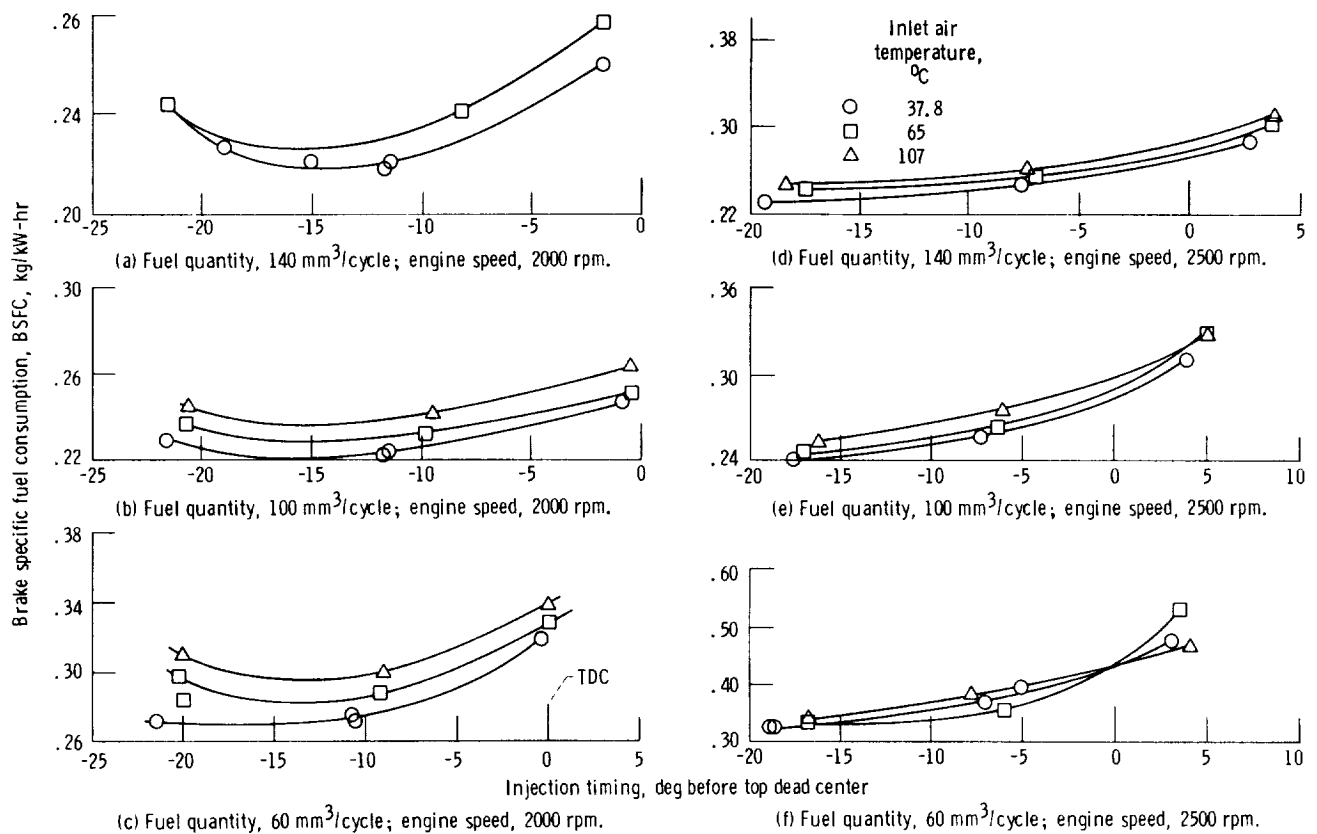
Figure 28. – Effect of inlet air temperature on BSFC. Inlet air pressure, 262 kPa.
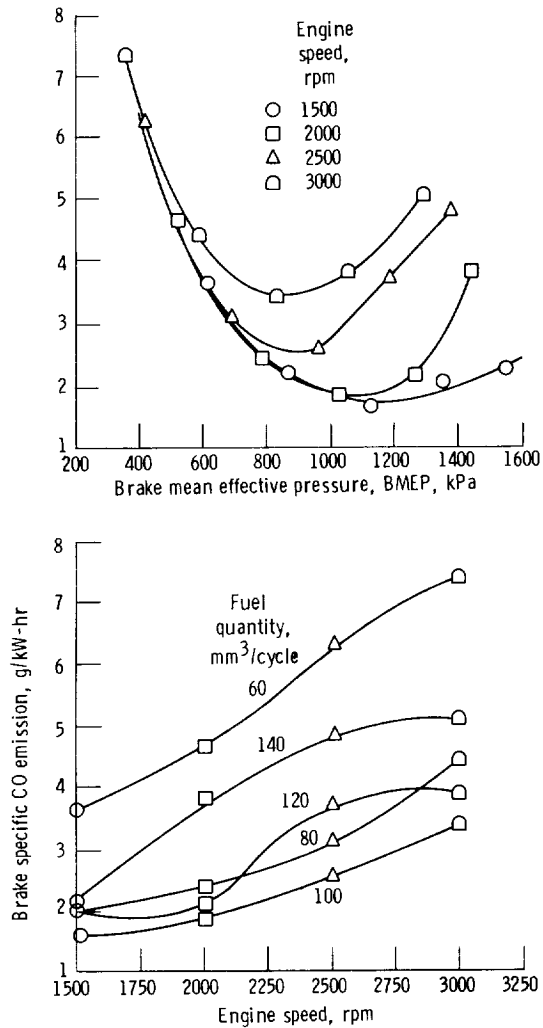
Figure 29. - Baseline carbon monoxide emissions. Engine optimized for performance. Inlet air temperature, 34° C; inlet air pressure, 262 kPa.
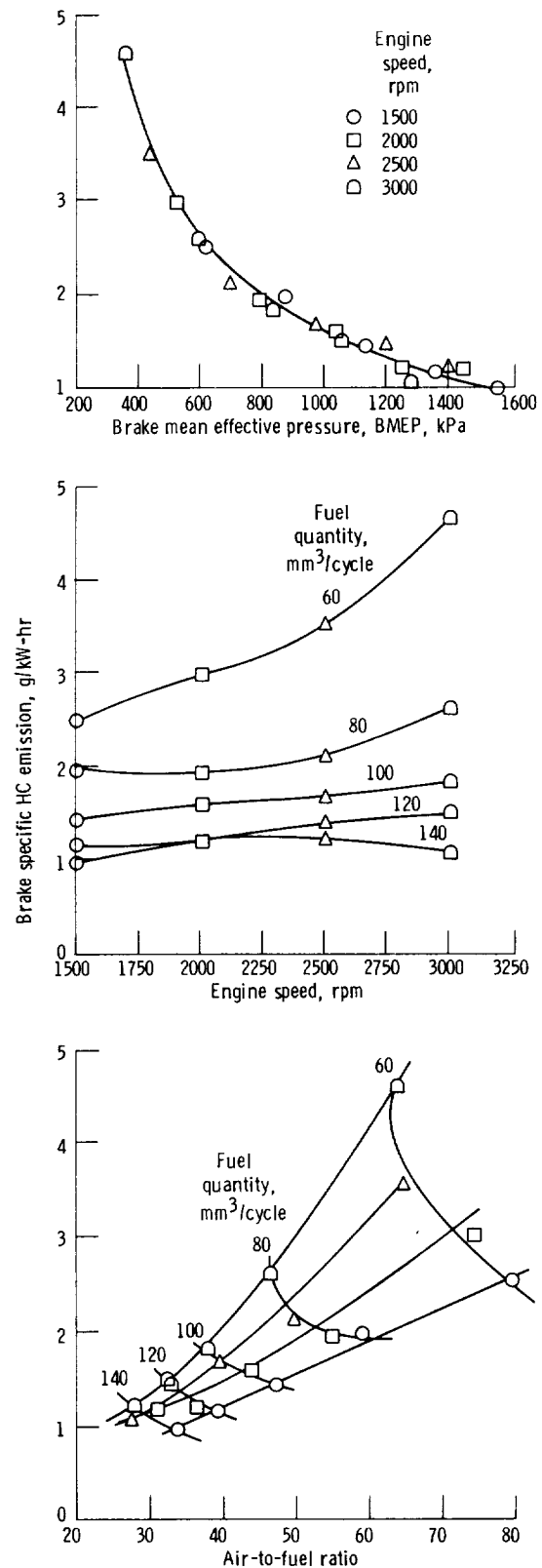
Figure 30. - Baseline hydrocarbon emissions. Engine optimized for performance. Inlet air temperature, 34° C; inlet air pressure, 262 kPa.
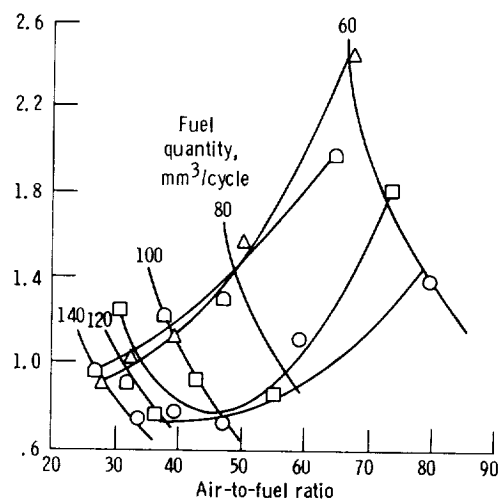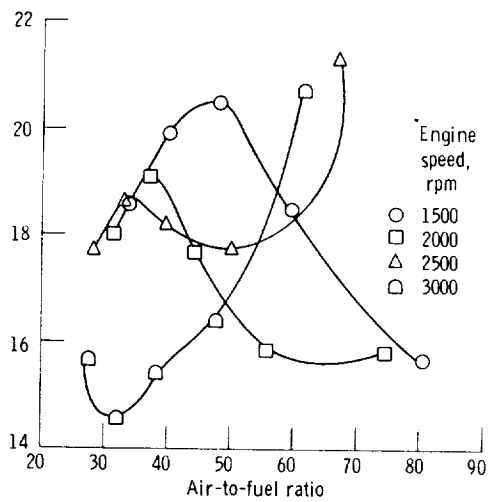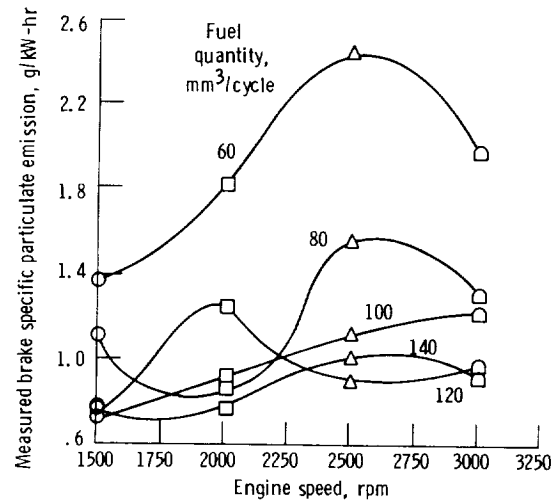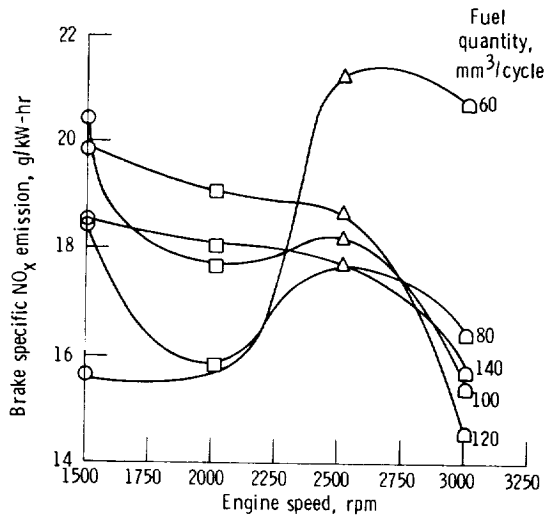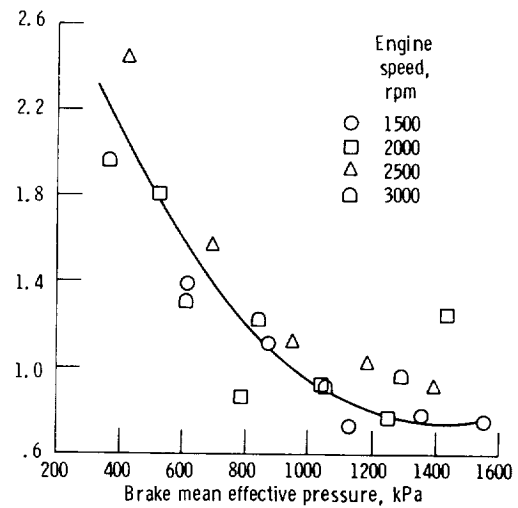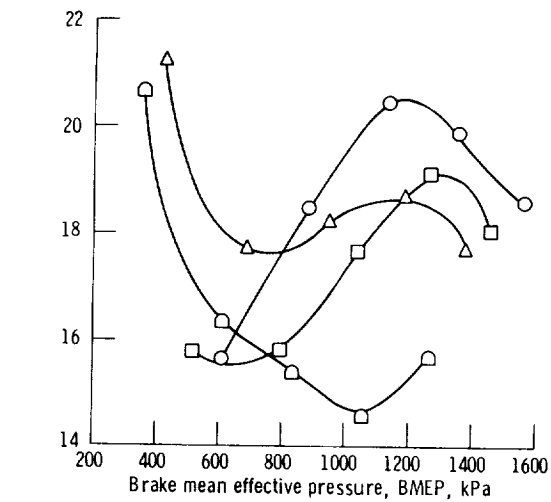
Figure 31. - Baseline oxides at nitrogen emissions. Engine optimized for performance. Inlet air temperature, 34° C; inlet air pressure, 262 kPa.

Figure 32. - Measured total particulate emissions. Engine optimized for performance. Inlet air temperature, 34° C; inlet air pressure, 262 kPa.
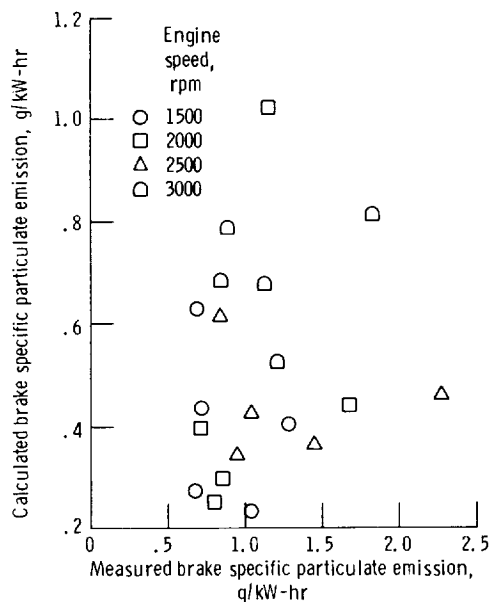
Figure 33. - Measured total particulates versus calculated particulates. Engine optimized for performance. Inlet air temperature, 34° C; inlet air pressure, 262 kPa.
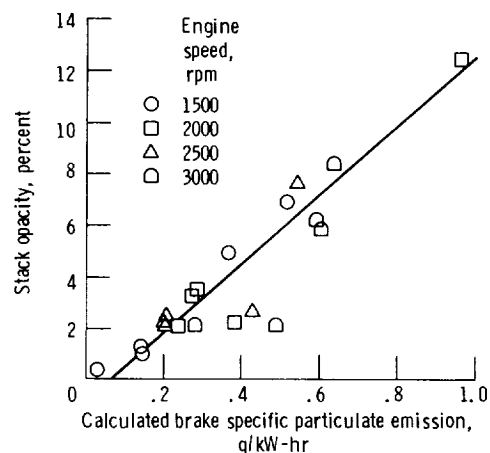
Figure 34. - Calculated brake specific particulate emissions versus percent smoke opacity. Inlet air temperature, 34° C; inlet air pressure, 262 kPa.
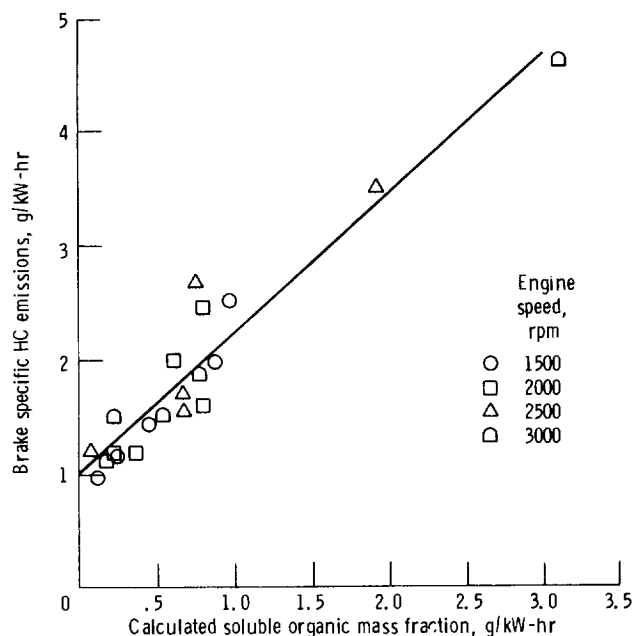
Figure 35. - Measured soluble organic fraction of total particulates versus hydrocarbon emissions.
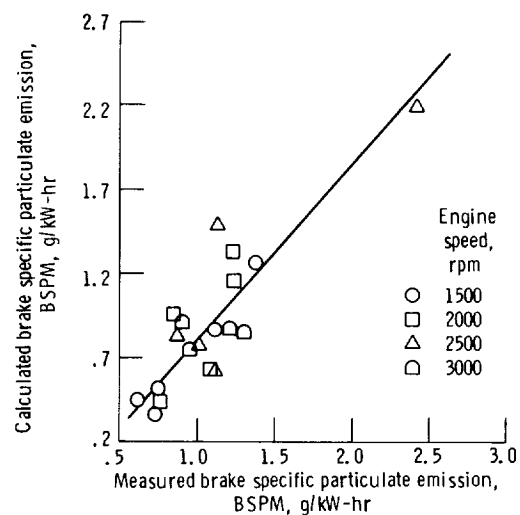
Figure 36. - Measured total particulates versus calculated total particulates (exhaust smoke opacity and total HC emissions).

Figure 38. - Effect of injection timing and inlet air temperature on emissions and BSFC. Fuel quantity, 120 mm^3/cycle; engine speed, 2500 rpm; inlet air temperature, 34^0 to 37^0 C.
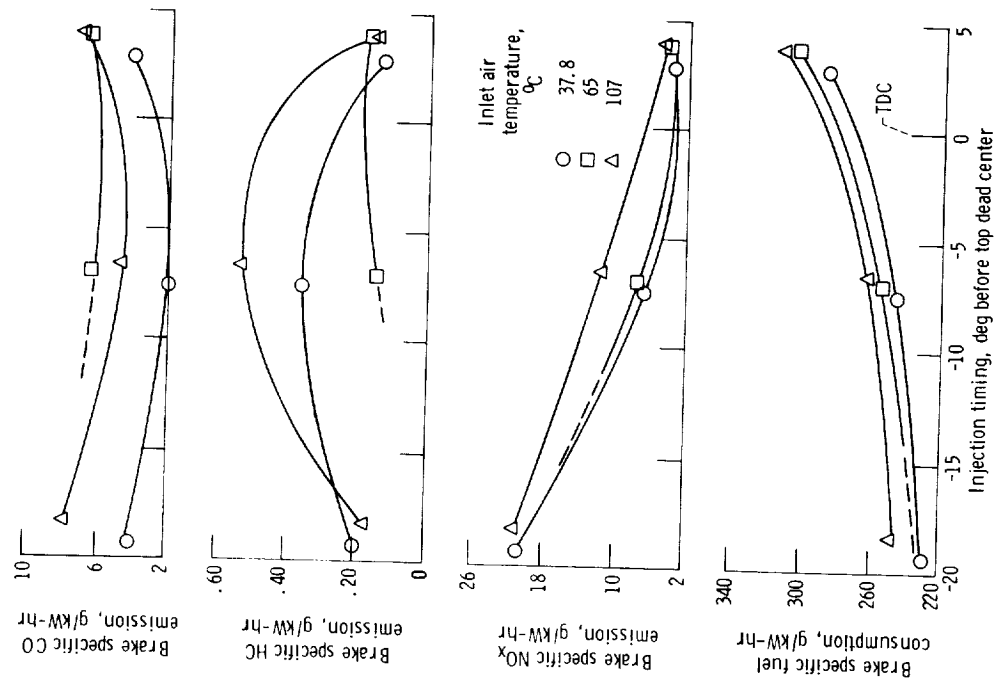
Figure 37. - Effect of injection timing and inlet air temperature on emissions and BSFC. Fuel quantity, 140 mm^3/cycle; engine speed, 2500 rpm; inlet air temperature, 34^0 to 37^0 C.

Figure 40. – Effect of injection timing and inlet air temperature on emissions and BSFC. Fuel quantity, 80 mm³/cycle; engine speed, 2500 rpm; inlet air temperature, 34° to 37° C.
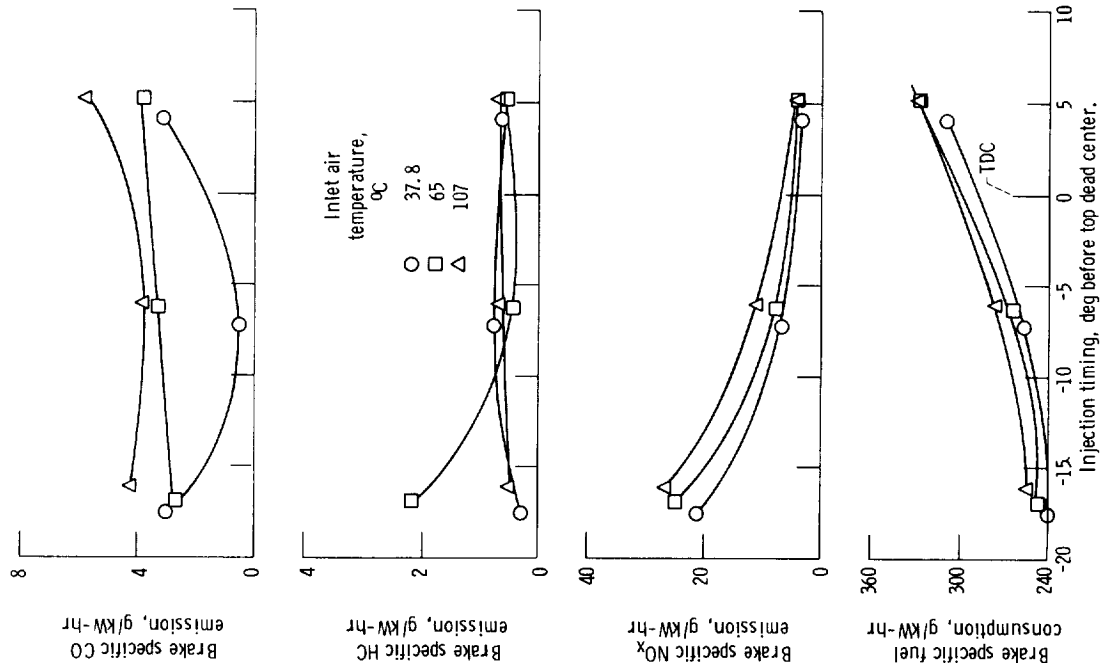
Figure 39. – Effect of injection timing and inlet air temperature on emissions and BSFC. Fuel quantity, 100 mm³/cycle; engine speed, 2500 rpm; inlet air temperature, 34° to 37° C.

Figure 42. - Effect of inlet air pressure on smoke opacity and gaseous emissions. Engine speed, 3000 rpm; inlet air temperature, 34° to 37° C.
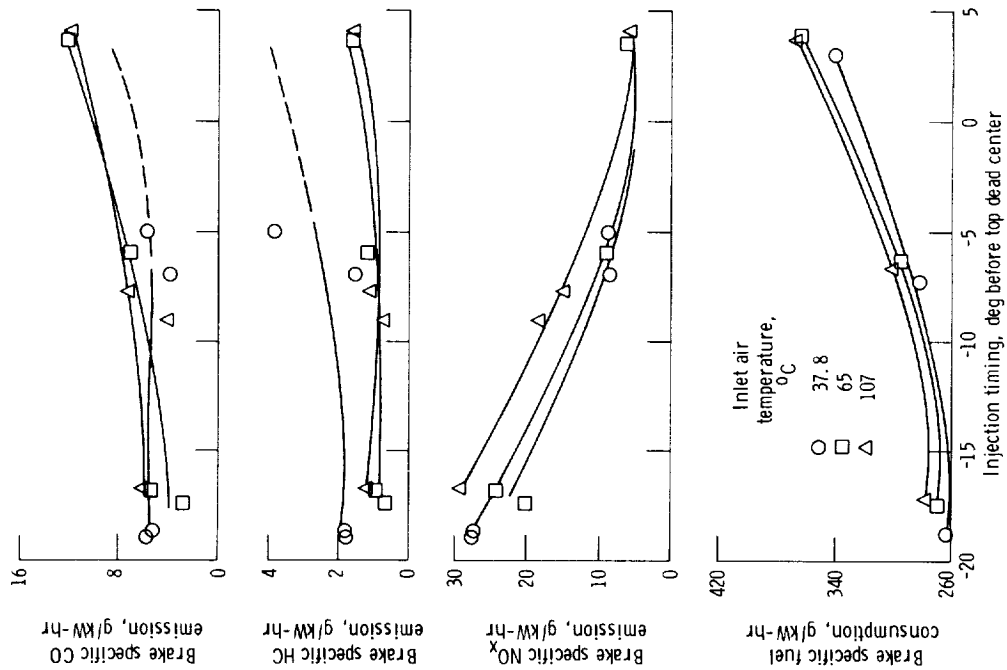
Figure 41. - Effect of injection timing and inlet air temperature on emissions and BSFC. Fuel quantity, 60 mm³/cycle; engine speed, 2500 rpm; inlet air temperature, 34° to 37° C.
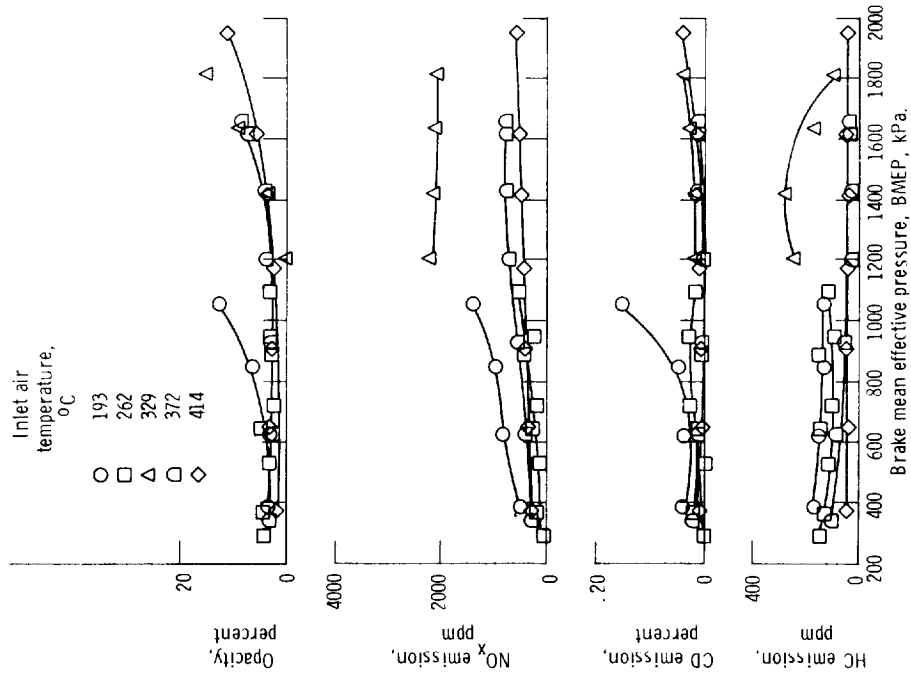
Figure 43. - Effect of inlet air pressure on smoke opacity and gaseous emissions. Engine speed, 2500 rpm; inlet air temperature, 340 to 370 C.
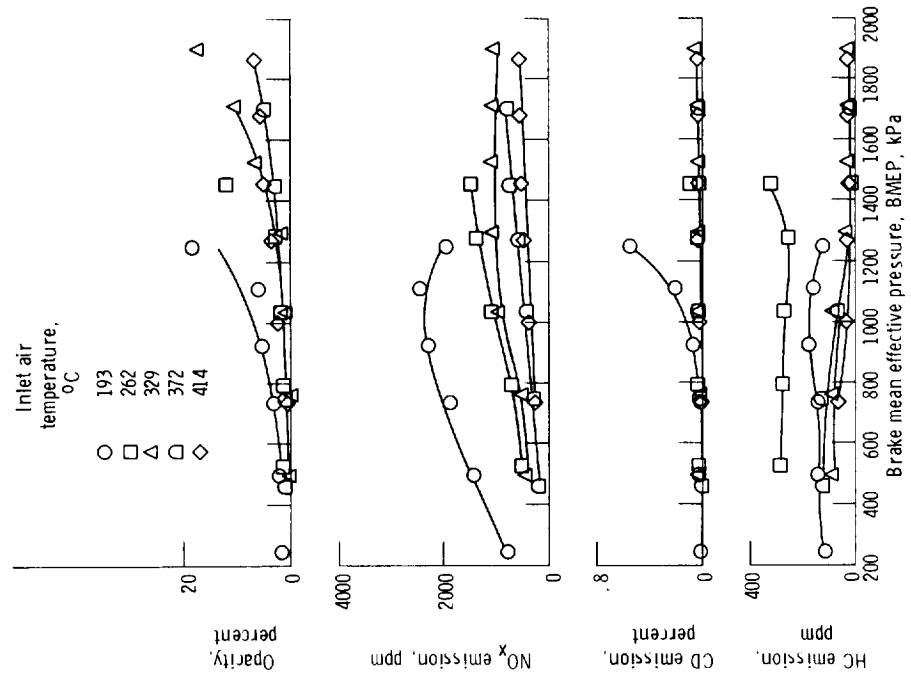
Figure 44. - Effect of inlet air pressure on smoke opacity and gaseous emissions. Engine speed, 2000 rpm; inlet air temperature, 340 to 370 C.
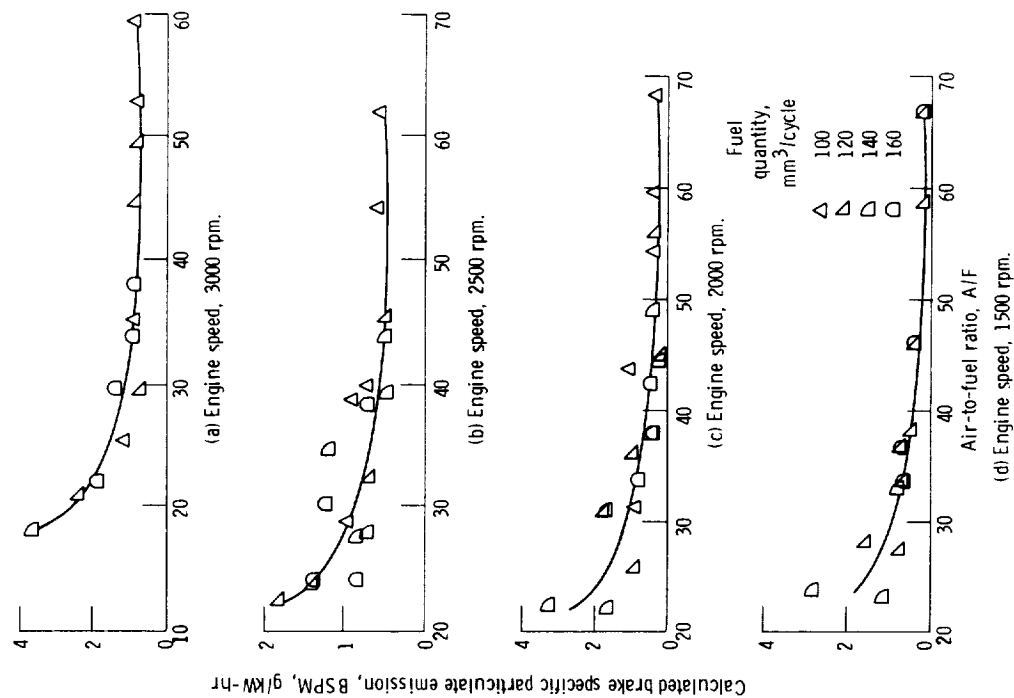
Figure 46. – Effect of A/F on total particulates (calculated).

(a) Engine speed, 3000 rpm.

(b) Engine speed, 2500 rpm.

(c) Engine speed, 2000 rpm.

(d) Engine speed, 1500 rpm.

Air-to-fuel ratio, A/F

Fuel quantity, mm³/cycle
100
120
140
160

Calculated brake specific particulate emission, BSPM, g/kW-hr
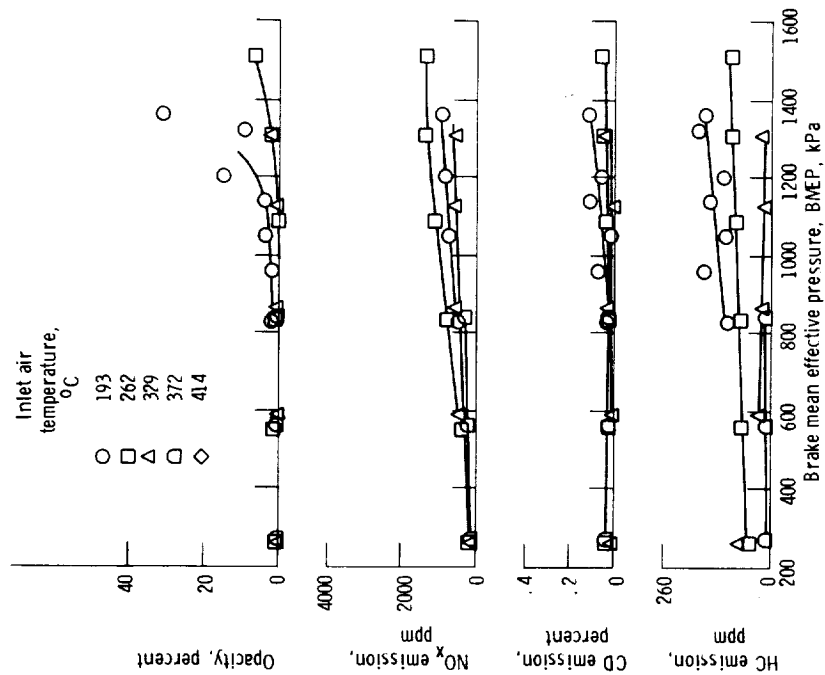
Figure 45. – Effect of inlet air pressure on smoke opacity and gaseous emissions. Engine speed, 1500 rpm; inlet air temperature, 34° to 37° C.

Brake mean effective pressure, BMEP, kPa

Inlet air temperature, °C
193
262
329
372
414

Opacity, percent

NOₓ emission, ppm

CO emission, percent

HC emission, ppm
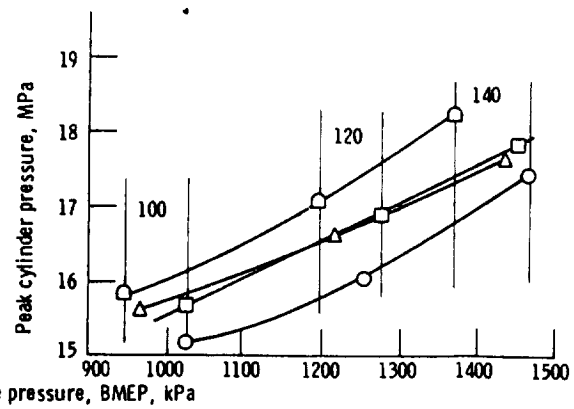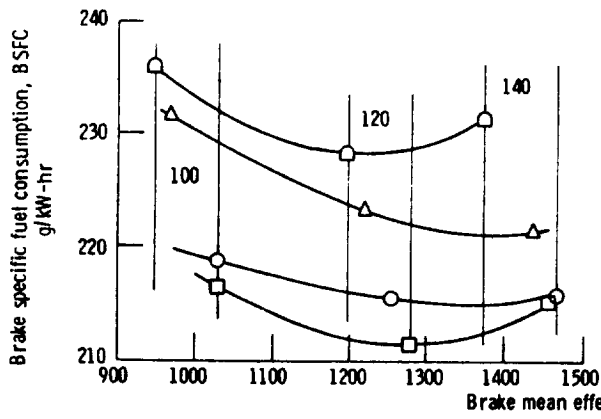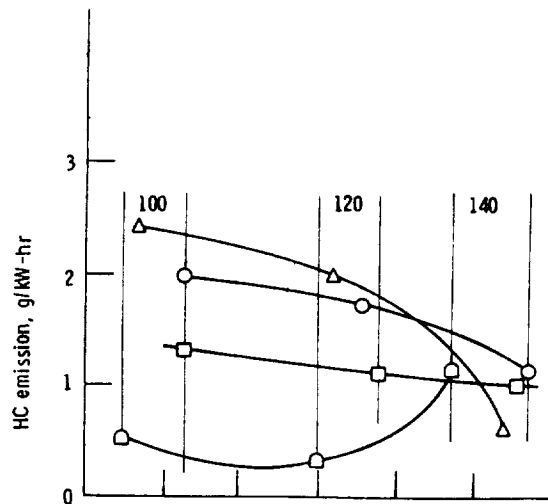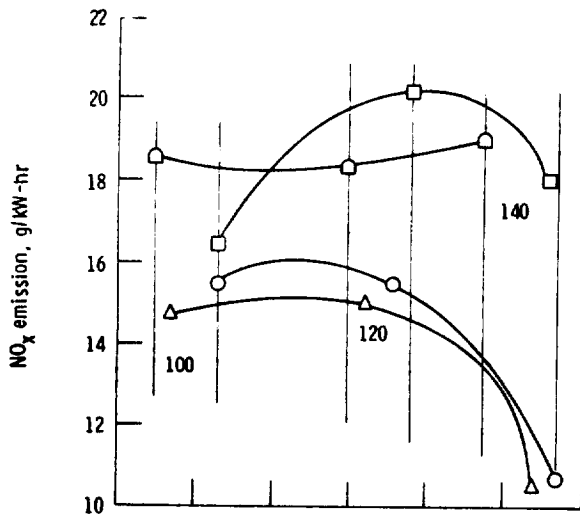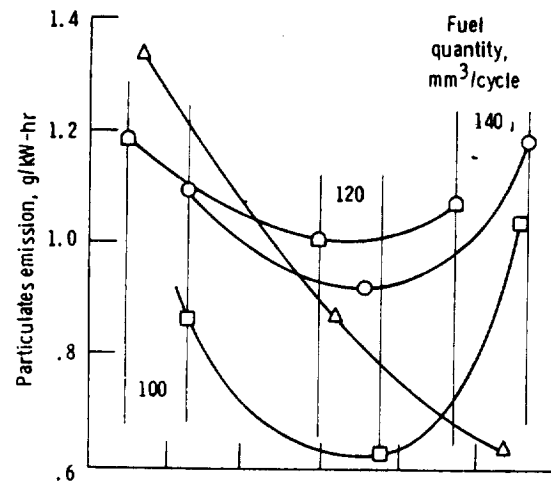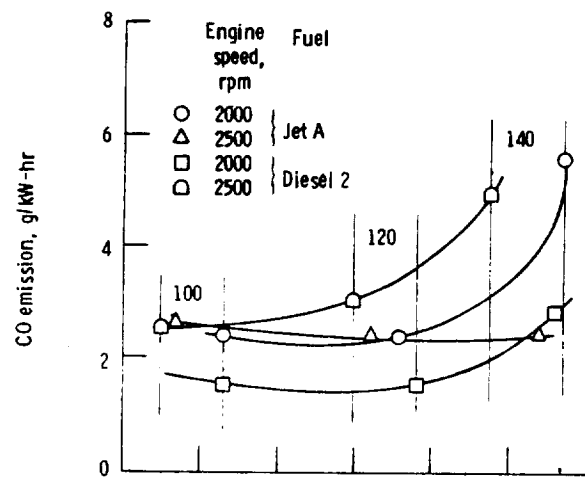
Figure 47. - Exhaust emissions and fuel consumption results with Jet A and diesel fuel.

Figure 49. – MEP in hot firing engine versus engine speed. Inlet air pressure, 262 kPa; exhaust pressure, 210 kPa.

Figure 48. – Mean effective pressures (IMEP$_u$) in hot firing engine versus engine speed. Inlet air pressure, 262 kPa; exhaust pressure, 210 kPa.
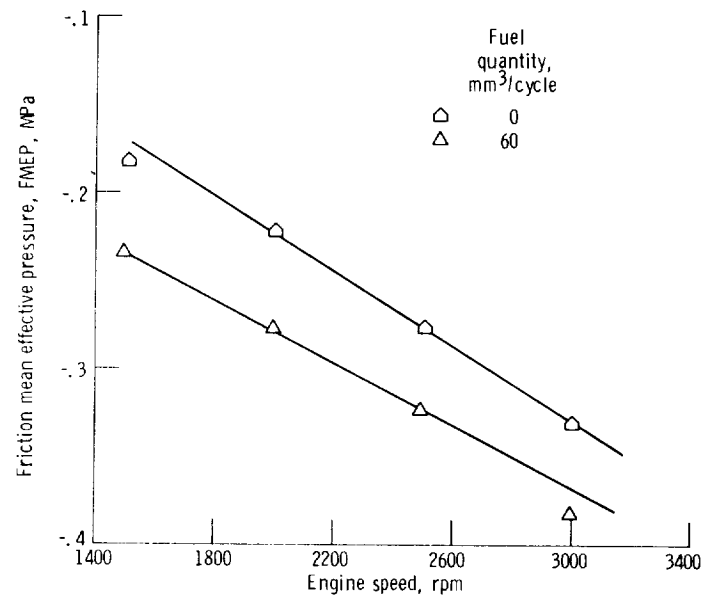
Figure 50. - FMEP values versus engine speed for a naturally aspirated
engine in both motored and hot firing operation.
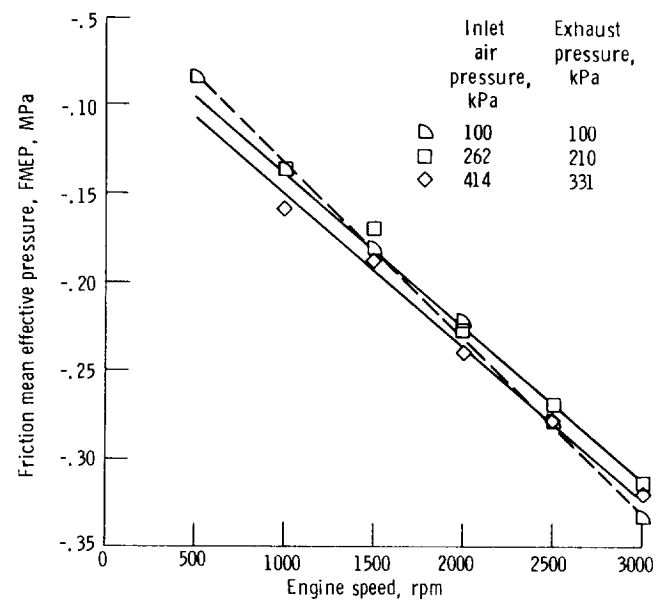
Figure 51. - FMEP versus engine speed for motored engine.
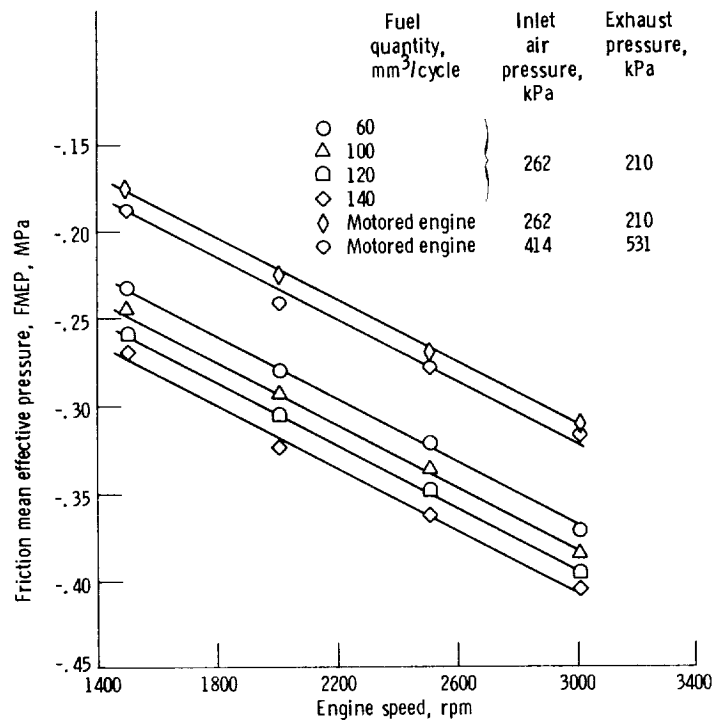
Figure 52. – FMEP values versus engine speed for hot firing engine.
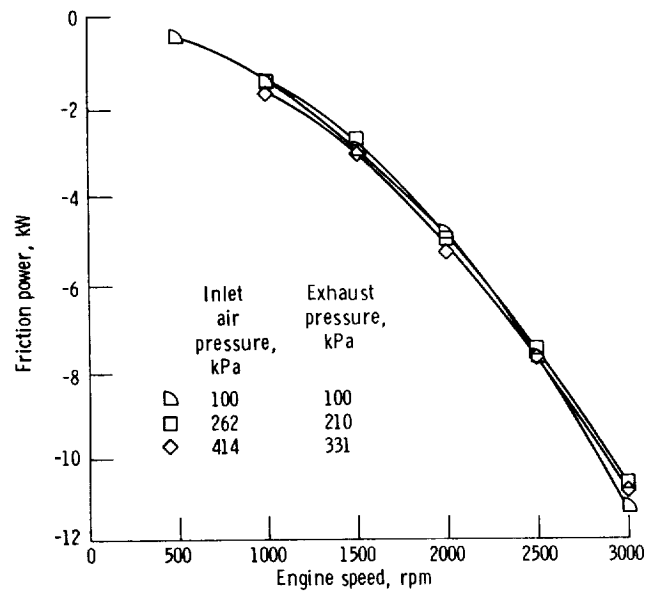
Figure 53. – Friction power equivalent for a motored engine operating at three inlet air pressures.
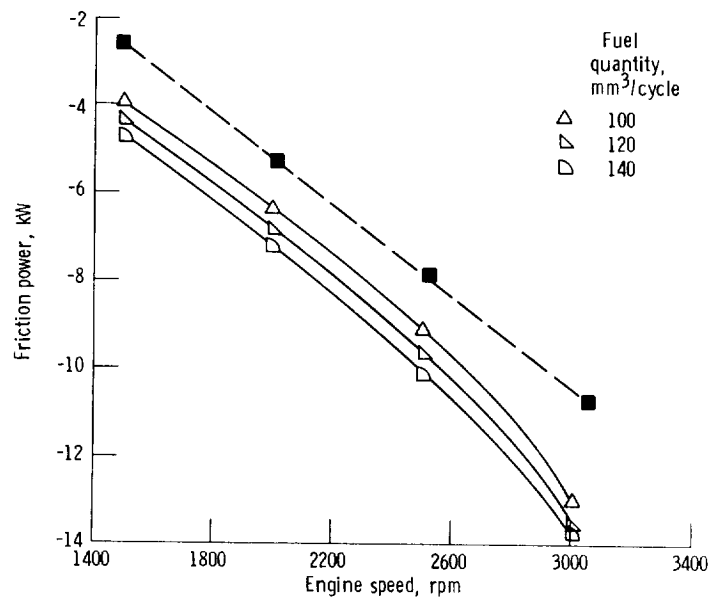
Figure 54. – Friction power for a hot firing engine operating under three loads. Inlet air pressure, 262 kPa; exhaust pressure, 210 kPa.
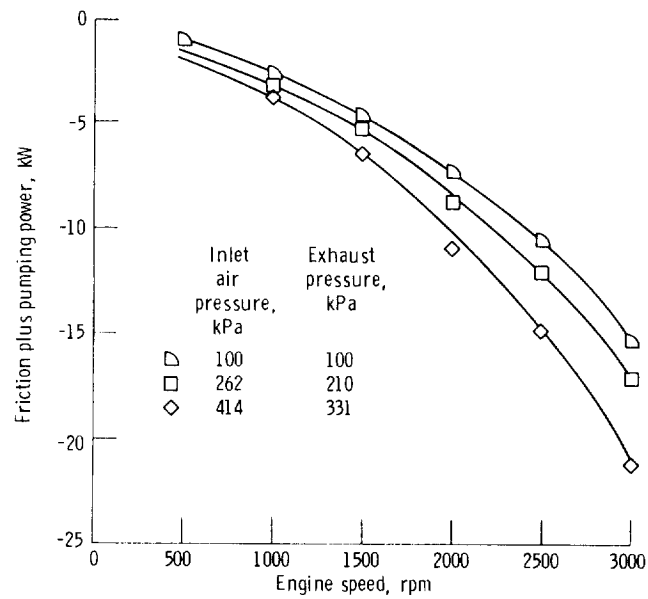
Figure 55. – Motored friction power plus pumping power versus engine speed for three inlet air pressure.
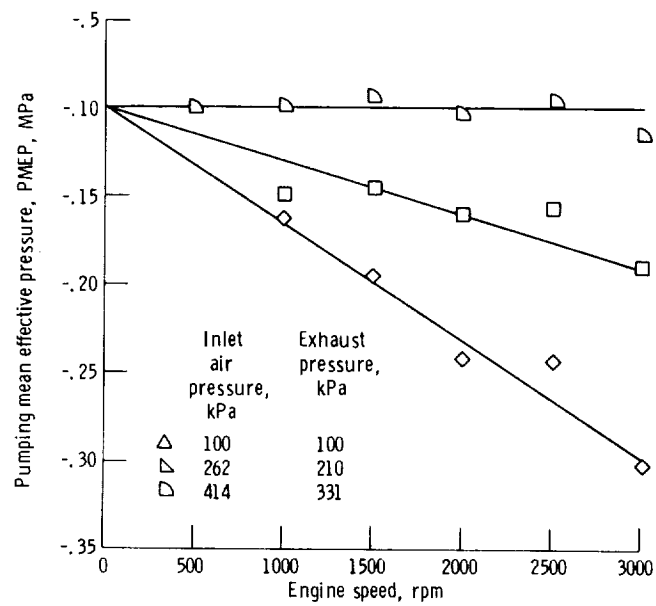
Figure 56. - PMEP values versus engine speed for motored engine operating at three inlet air pressures.
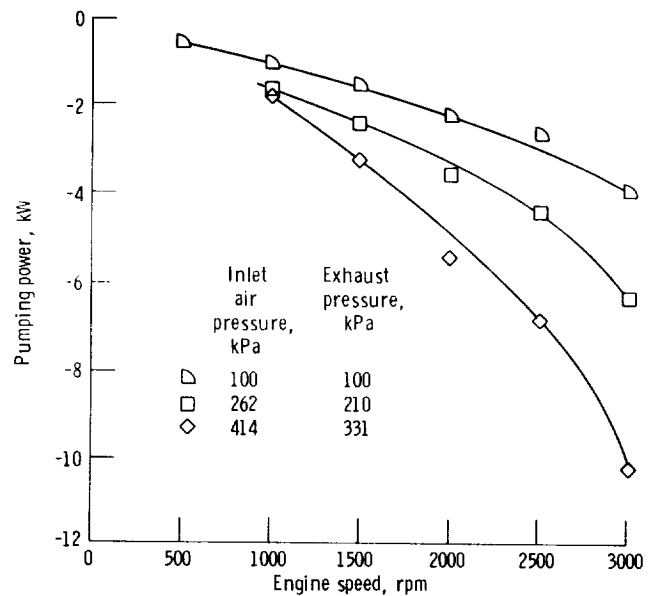
Figure 57. - Pumping power losses versus engine speed for motored engine operating at three inlet air pressures.

Fuel quantity, mm³/cycle	Inlet air pressure, kPa	Exhaust pressure, kPa	Engine operating mode
0	100	100	Motored
0	262	210	Motored
100			
120	262	210	Firing
140			
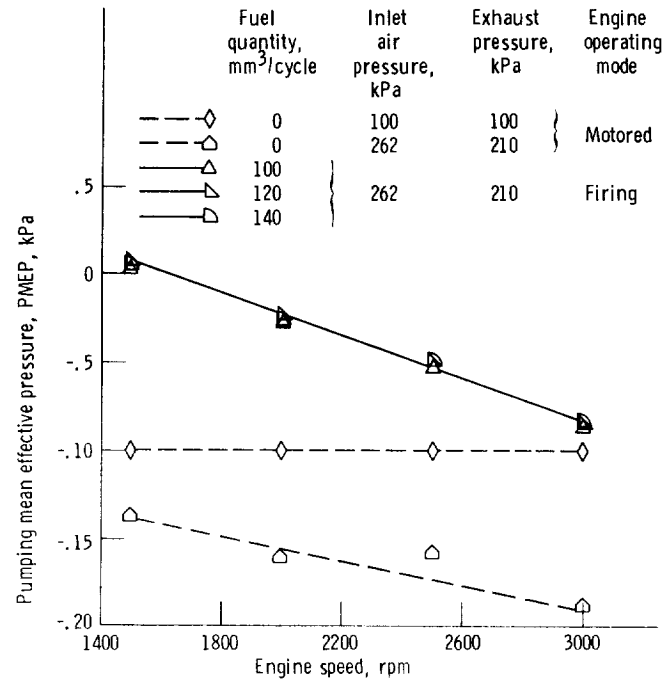
Figure 58. - Comparison of PMEP for an engine under motored and under hot firing conditions.

Fuel quantity, mm³/cycle	Inlet air pressure, kPa	Exhaust pressure, kPa	Engine operating mode
0	100	100	Motored
0	262	210	Motored
0	414	331	Motored
100			
120	262	210	Firing
140			
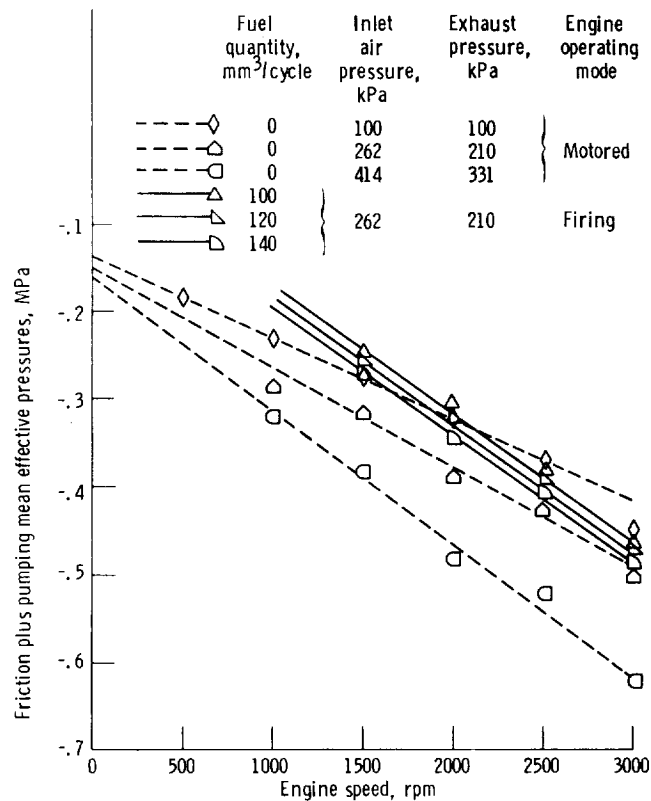
Figure 59. - Combined FMEP and PMEP losses from a motored engine compared with operation of the engine under load.
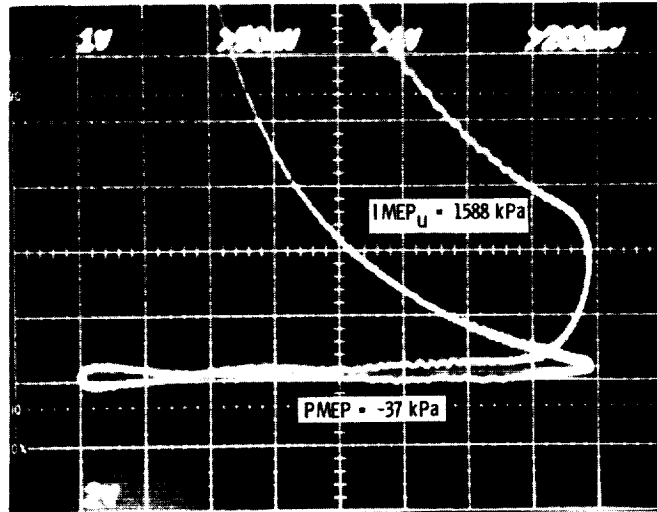
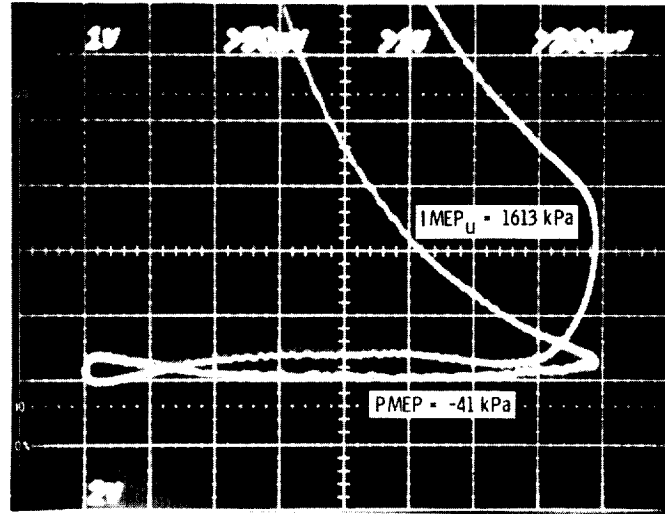(a) Brake specific fuel consimption, 218 g/kW-hr; inlet to exhaust pressure ratio, 1.25.
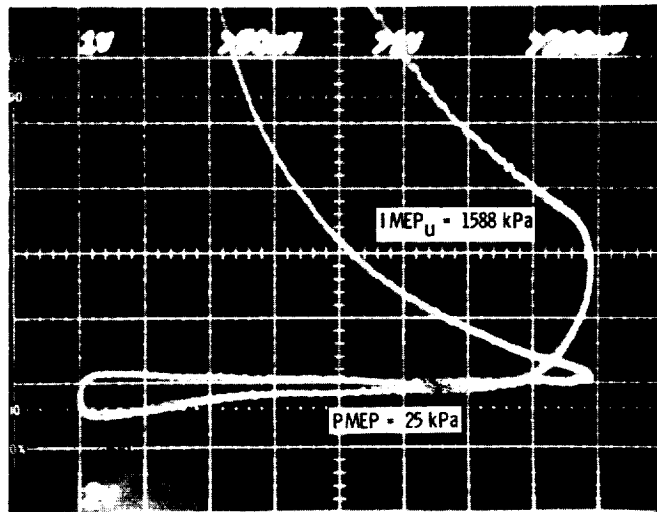
(b) Brake specific fuel consimption, 208 g/kW-hr; inlet to exhaust pressure ratio, 1.72.
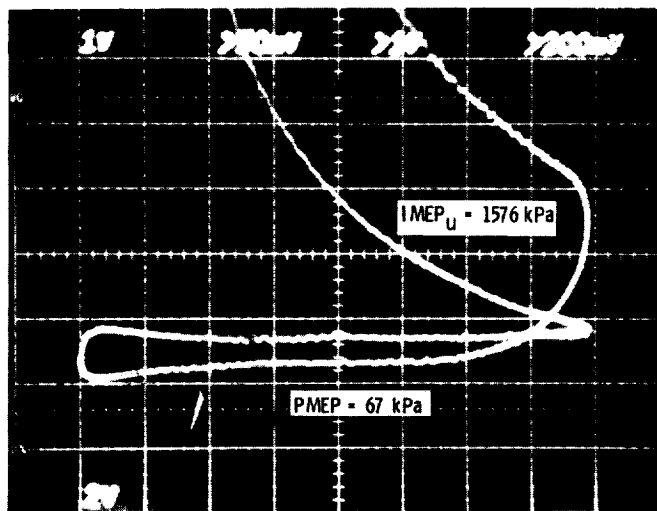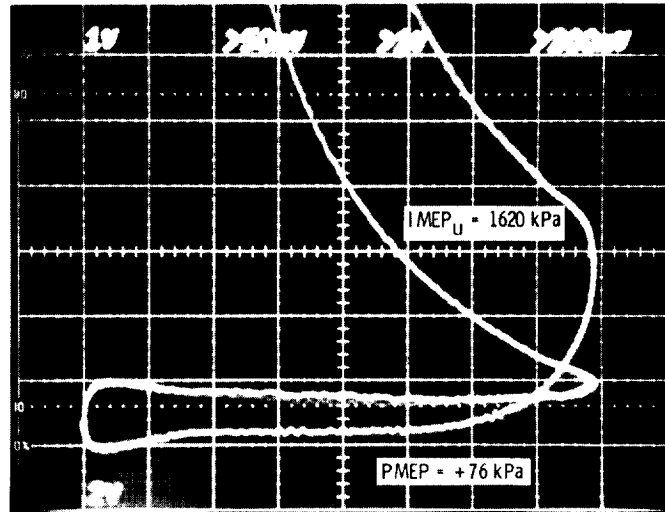

(c) Brake specific fuel consimption, 203 g/kW-hr; inlet to exhaust pressure ratio, 2.40.
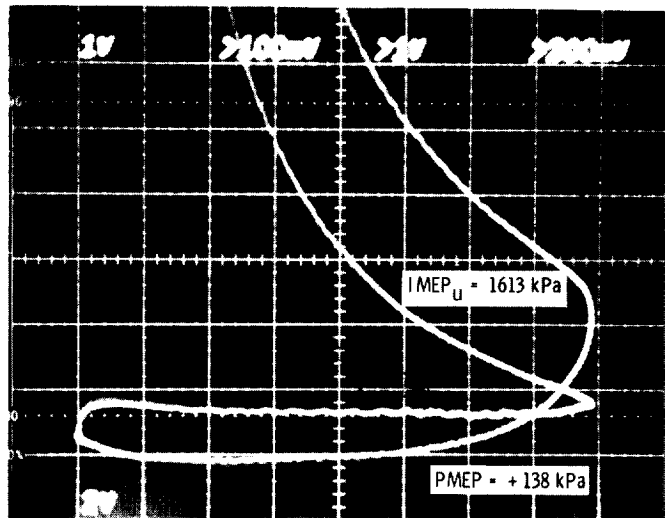
Figure 60. - Pumping loop diagrams. Inlet air pressure, 262 kPa; engine speed, 2000 rpm; fuel quantity, 120 mm^3/cycle.

(a) Brake specific fuel consumption, 213 g/kW-hr; inlet to exhaust pressure ratio, 1.25.

(b) Brake specific fuel consumption, 195 g/kW-hr; inlet to exhaust pressure ratio, 2.00.

(c) Brake specific fuel consimption, 188 g/kW-hr; inlet to exhaust pressure ratio, 3.33.

Figure 61. - Pumping loop diagrams. Inlet air pressure, 414 kPa; engine speed, 2000 rpm; fuel quantity, 120 mm^3/cycle.
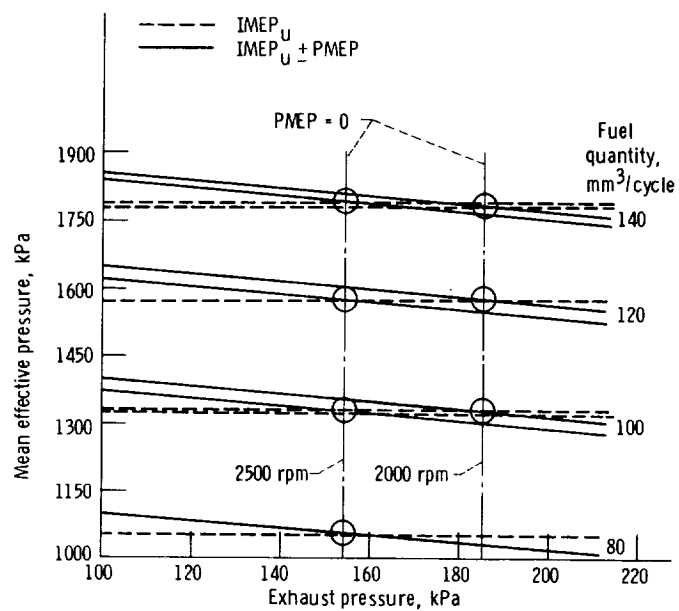
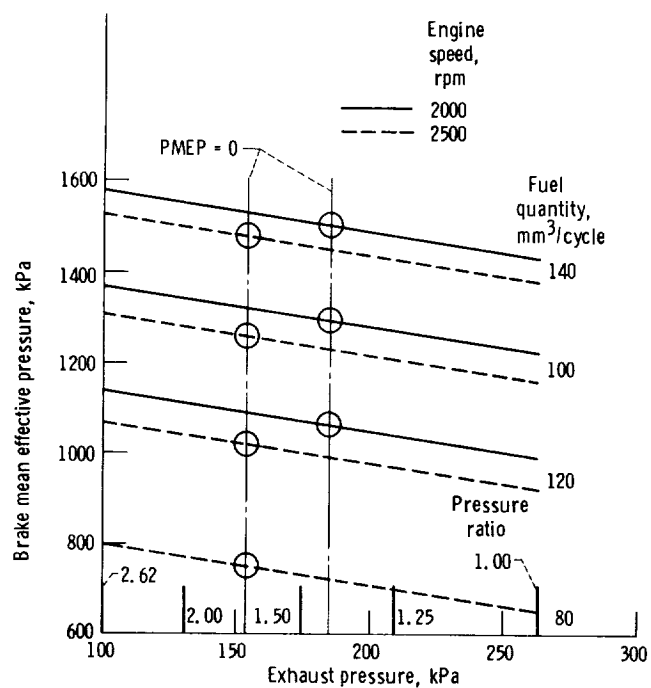Figure 62. – Effect of exhaust backpressure on mean effective
pressures.

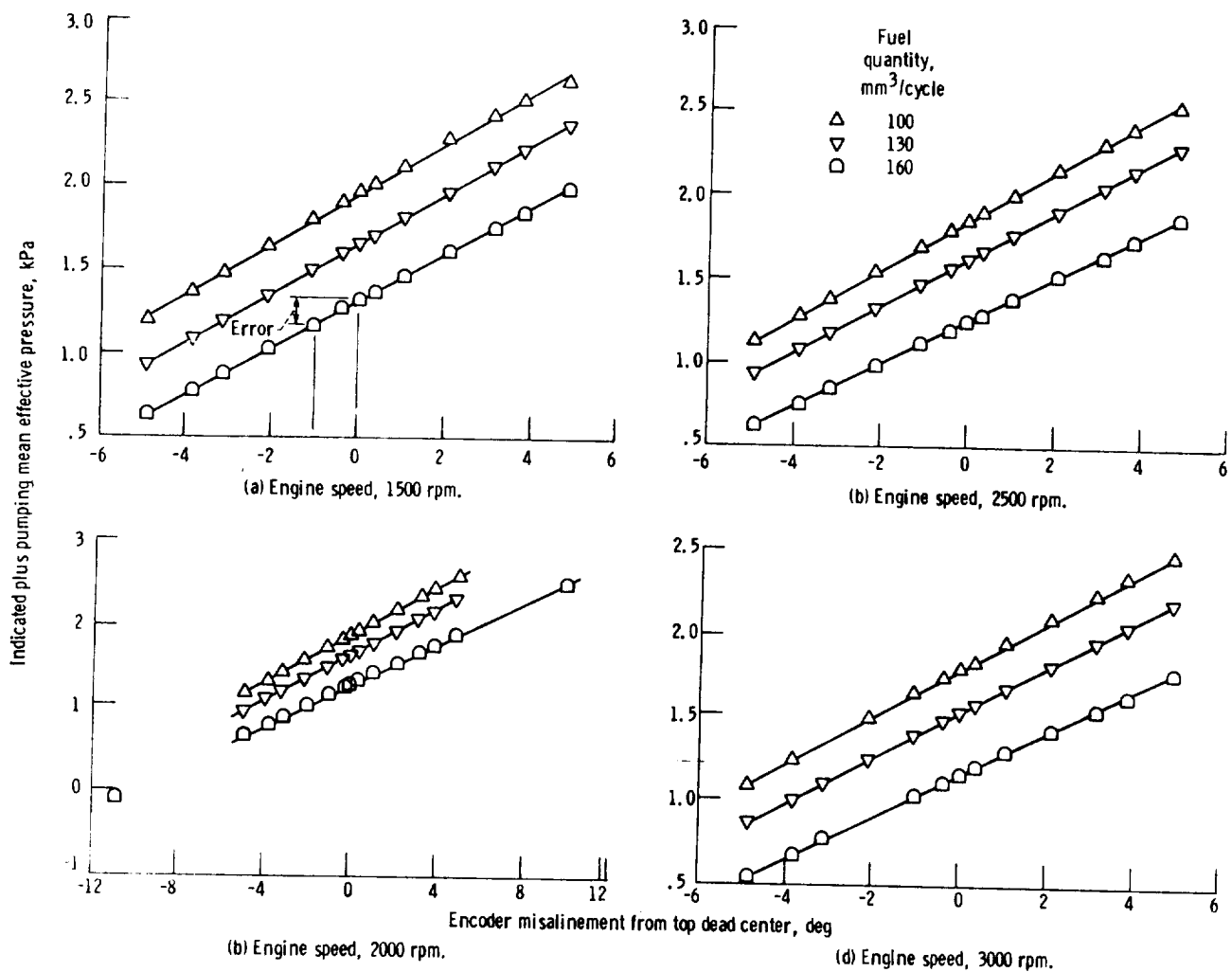Figure 63. – Effect of exhaust backpressure on BMEP.

Figure 64. – Effects of encoder misalinement on net values of upper loop IMEP. Inlet air pressure, 262 kPa; inlet-to-exhaust pressure ratio, 1.25

1. Report No. NASA TM- 86873	2. Government Accession No.	3. Recipient's Catalog No.

4. Title and Subtitle	5. Report Date
Baseline Performance and Emissions Data for a Single-Cylinder, Direct-Injected, Diesel Engine	August 1984
	6. Performing Organization Code 505-40-62

7. Author(s)	8. Performing Organization Report No.
Robert A. Dezelick, John J. McFadden, Lloyd W. Ream, and Richard F. Barrows	
	10. Work Unit No. E-2079

9. Performing Organization Name and Address	11. Contract or Grant No.
National Aeronautics and Space Administration Lewis Research Center Cleveland, Ohio 44135	
	13. Type of Report and Period Covered Technical Memorandum

12. Sponsoring Agency Name and Address	
U.S. Department of Energy Office of Vehicle and Engine R&D Washington, D.C. 20585	14. Sponsoring Agency Code Report No. DOE/NASA/50194-38

16. Abstract

This report documents comprehensive fuel consumption, mean effective cylinder pressure, and emission test results for a supercharged, single-cylinder, direct-injected, four-stroke-cycle, diesel test engine. Inlet air-to-exhaust pressure ratios were varied from 1.25 to 3.35 in order to establish the potential effects of turbocharging techniques on engine performance. Inlet air temperatures and pressures were adjusted from 34^0 to 107^0 C and from 193 to 414 kPa to determine the effects on engine performance and emissions. Engine output ranged from 300 to 2100 kPa (brake mean effective pressure) in the speed range of 1000 to 3000 rpm. Gaseous and particulate emission rates were measured. Real-time values of engine friction and pumping loop losses were measured independently and compared with motored engine values.

17. Key Words (Suggested by Author(s))	18. Distribution Statement
Diesel, Fuel consumption, Emissions, Particulates, Turbocharged diesel, Pumping loss, Turbocompound, Fuel injection, Friction loss	Unclassified - Unlimited Star Category 85 DOE Category UC-96

19. Security Classif. (of this report)	20. Security Classif. (of this page)	21. No. of pages	22. Price*
Unclassified	Unclassified	29	A03

National Aeronautics and
Space Administration

Washington, D.C.
20546

SPECIAL FOURTH CLASS MAIL
BOOK

U.S.MAIL

NASA

POSTMASTER: If Undeliverable (Section 158
Postal Manual) Do Not Return